JCI The Journal of Clinical Investigation

Reduced expression of phosphatase PTPN2 promotes pathogenic conversion of Tregs in autoimmunity

Mattias N.D. Svensson, … , Pandurangan Vijayanand, Nunzio Bottini

J Clin Invest. 2019. https://doi.org/10.1172/JCI123267.

Research In-Press Preview **Autoimmunity** **Immunology**

Genetic variants at the *PTPN2* locus, which encodes the tyrosine phosphatase PTPN2, cause reduced gene expression and are linked to rheumatoid arthritis (RA) and other autoimmune diseases. PTPN2 inhibits signaling through the T cell and cytokine receptors and loss of PTPN2 promotes T cell expansion and CD4 and CD8-driven autoimmunity. However, it remains unknown whether loss of PTPN2 in FoxP3$^+$ regulatory T cells (Treg) plays a role in autoimmunity. Here we aimed to model human autoimmune-predisposing *PTPN2* variants, which results in a partial loss of*PTPN2* expression, in mouse models of RA. We identified that reduced expression of *Ptpn2* enhanced the severity of autoimmune arthritis in the T cell dependent SKG mouse model and demonstrated that this phenotype was mediated through a Treg-intrinsic mechanism. Mechanistically, we found that through dephosphorylation of STAT3, Ptpn2 inhibits IL-6-driven pathogenic loss of FoxP3 after Tregs have acquired RORγt expression, at a stage when chromatin accessibility for STAT3-targeted IL-17 associated transcription factors is maximized. We conclude that PTPN2 promotes FoxP3 stability in mouse RORγt$^+$ Tregs and that loss of function of *PTPN2* in Tregs contributes to the association between PTPN2 and autoimmunity.

Reduced expression of phosphatase PTPN2 promotes pathogenic conversion of Tregs in autoimmunity

Mattias N.D. Svensson[1,2], Karen M. Doody[2], Benjamin J. Schmiedel[3], Sourya Bhattacharyya[3], Bharat Panwar[3], Florian Wiede[4], Shen Yang[1], Eugenio Santelli[1], Dennis J. Wu[1,2], Cristiano Sacchetti[1,2], Ravindra Gujar[3], Gregory Seumois[3], William B. Kiosses[5], Isabelle Aubry[6], Gisen Kim[7], Piotr Mydel[8,9], Shimon Sakaguchi[10,11], Mitchell Kronenberg[7], Tony Tiganis[4,12,13], Michel L. Tremblay[6], Ferhat Ay[3], Pandurangan Vijayanand[3] and Nunzio Bottini[1,2*]

[1]Department of Medicine, University of California, San Diego, La Jolla, CA, USA

[2]Division of Cellular Biology, La Jolla Institute for Allergy and Immunology, La Jolla, CA, USA

[3]Division of Vaccine Discovery, La Jolla Institute for Allergy and Immunology, La Jolla, CA, USA

[4]Peter MacCallum Cancer Centre, Melbourne, Victoria, 3000, Australia

[5]Core Microscopy, La Jolla Institute for Allergy and Immunology, La Jolla, CA, USA

[6]Department of Biochemistry, McGill University, Montréal, QC, Canada

[7]Division of Developmental Immunology, La Jolla Institute for Allergy and Immunology, La Jolla, CA, USA

[8]Clinical Science, Broegelmann Research Laboratory, Bergen, Norway

[9]Department of Microbiology, Jagiellonian University, Krakow, Poland

[10]Laboratory of Experimental Immunology, Immunology Frontier Research Center, Osaka University, Suita, Japan

[11]Department of Experimental Pathology, Institute for Frontier Medical Sciences, Kyoto University, Kyoto, Japan

[12]Monash Biomedicine Discovery Institute, Monash University, Clayton, Victoria 3800, Australia

[13]Department of Biochemistry and Molecular Biology, Monash University, Clayton, Victoria 3800, Australia

*Corresponding author: Nunzio Bottini, MD, PhD, Department of Medicine, University of California San Diego, ACTRI, 9452 Medical Center Dr., La Jolla, CA 92037, Phone: +1 (858) 246-2398, Email: nbottini@ucsd.edu

Conflict of interest statement: no conflict of interest exists

Abstract

Genetic variants at the *PTPN2* locus, which encodes the tyrosine phosphatase PTPN2, cause reduced gene expression and are linked to rheumatoid arthritis (RA) and other autoimmune diseases. PTPN2 inhibits signaling through the T cell and cytokine receptors and loss of PTPN2 promotes T cell expansion and CD4 and CD8-driven autoimmunity. However, it remains unknown whether loss of PTPN2 in FoxP3$^+$ regulatory T cells (Treg) plays a role in autoimmunity. Here we aimed to model human autoimmune-predisposing *PTPN2* variants, which results in a partial loss of *PTPN2* expression, in mouse models of RA. We identified that reduced expression of *Ptpn2* enhanced the severity of autoimmune arthritis in the T cell dependent SKG mouse model and demonstrated that this phenotype was mediated through a Treg-intrinsic mechanism. Mechanistically, we found that through dephosphorylation of STAT3, *Ptpn2* inhibits IL-6-driven pathogenic loss of FoxP3 after Tregs have acquired RORγt expression, at a stage when chromatin accessibility for STAT3-targeted IL-17 associated transcription factors is maximized. We conclude that PTPN2 promotes FoxP3 stability in mouse RORγt$^+$ Tregs and that loss of function of PTPN2 in Tregs contributes to the association between *PTPN2* and autoimmunity.

Introduction

Rheumatoid arthritis (RA) is a chronic autoimmune, systemic inflammatory disorder that primarily affects diarthrodial joints(1). To date, various genome-wide association studies (GWAS) have identified over 100 risk loci for RA(2, 3). One gene found to be highly associated with RA is *PTPN2*, which encodes for the protein tyrosine phosphatase (PTP) PTPN2, also known as T cell PTP(2). PTPN2 also strongly associates with inflammatory bowel disease (IBD)(4). Homozygous carriage of the risk allele at the rs1893217 SNP - that tags an autoimmunity-associated *PTPN2* haplotype - results in a 33-50% decrease in *PTPN2* mRNA in human $CD4^+$ memory T cells(5). Also, the same rs1893217 risk allele drove reduced PTPN2 protein expression and acted as a loss-of-function variant when transfected into THP-1 cells(6).

PTPN2 is a ubiquitously expressed PTP and in hematopoietic cells it works as an important negative regulator of T cell receptor (TCR) and cytokine signaling by dephosphorylating SRC family kinases Lck and Fyn, Janus-activating kinases (JAK)-1 and -3 and Signaling transducer and activators of transcription (STATs)-1, 3 and 5(7-11).

How loss of function of PTPN2 promotes risk of RA and other autoimmune diseases is incompletely understood. However, the importance of PTPN2 in inflammation is exemplified by the fact that global deletion of *Ptpn2* in mice leads to early lethality due to progressive systemic myeloid-cell driven inflammation(12). Further experiments with mice carrying conditional deletion of *Ptpn2* demonstrated that PTPN2 also plays a critical role in maintenance of T cell tolerance. Mice carrying T cell specific deletion of *Ptpn2* showed enhanced TCR signaling, altered thymic selection and increased proliferation of peripheral T cells, together resulting in CD8-driven systemic autoimmunity(9). Complete *Ptpn2* deficiency in T cells also favored CD4 polarization towards a Th1 and Th17 fate, promoting aggressive colitis(13), which correlated with increased Th1 and Th17 marker expression in inflamed colon tissue from Crohn's disease (CD) patients carriers of rs1893217(13).

Although these studies point to a role of PTPN2 in modulation of T cell tolerance, it remains unclear how loss of function of PTPN2 affects autoimmunity-protective FoxP3^{+} regulatory T cells (Treg)(14, 15). Two studies showing that complete knockout (KO)(9, 10) of *Ptpn2* promotes Treg expansion and FoxP3 stabilization in induced Tregs (iTreg)(16) suggest that loss of function of *Ptpn2* in Treg might partially counterbalance the autoimmunity risk induced by *Ptpn2* KO in FoxP3 negative CD4 and CD8 T cells. However, the role of PTPN2 or other tyrosine phosphatases in Tregs has yet to be addressed through cell-specific genetic manipulation.

In the present study, aimed to model the effect of partial loss of function of *PTPN2* in autoimmunity-prone human carriers, we assessed whether haploinsufficiency of *Ptpn2* enhances severity of disease in multiple models of RA. We show that *Ptpn2* haploinsufficiency promotes CD4-driven autoimmune arthritis. Unexpectedly, we found that partial loss of function of *Ptpn2* in Tregs promotes autoimmunity by destabilizing FoxP3 expression in the context of arthritis-induced inflammation.

Results

PTPN2 haploinsufficiency promotes T cell-mediated arthritis

Figures 1A-C shows an in silico assessment of the extent of overlap between RA-associated SNPs and DNase I hypersensitivity sites (DHS) and active histone marks in the *PTPN2* locus for different immune cell types. This type of analysis is useful to get insight about the key cellular players where the *PTPN2* locus selectively harbors a higher number of *cis*-regulatory DNA elements (DHS) and thus are most likely to be perturbed by the RA-associated SNPs(17). We found that the *PTPN2* locus shows distinct patterns of DHS and histone modifications in CD4 T cells as compared to B cells and monocytes (Figure 1A and Supplemental Figure 1A), suggesting that the locus is more accessible and active in T cells. CD4 memory T cells were particularly enriched for DHS within the *PTPN2* locus (Figure 1B). RA-associated *PTPN2* SNPs that directly overlap with DHS were also enriched in CD4 T cells, overall pointing to CD4 T cells as the key cellular target of *PTPN2*-dependent pathogenesis of RA (Figure 1C).

Since PTPN2 regulates important functions in innate immune cells such as macrophages and in synovial fibroblasts(7, 18), we first subjected *Ptpn2*$^{+/+}$ and *Ptpn2*$^{+/-}$ BALB/c mice to K/BxN passive serum transfer and collagen antibody-induced arthritis (CAIA), two models dependent on innate immune cells (19-22). In these models, *Ptpn2* haploinsufficiency did not affect development of arthritis (Figure 1D and Supplemental Figure 1B, C), suggesting that partial loss of function of *Ptpn2* does not enhance the arthritogenic action of innate immune cells.

We next evaluated the effect of *Ptpn2* haploinsufficiency in the SKG model of autoimmune arthritis. The *Zap70*^{SKG} (W163C) mutation results in altered thymic selection and emergence of self-reactive T cells that in the context of the H-2^{d} haplotype, result in Th17 cell dependent spontaneous arthritis (23, 24). Partial loss of function of *Ptpn2* significantly increased spontaneous development of arthritis in female SKG mice (Figure 1E), with increased cartilage depletion and bone damage (Supplemental Figure 1D, E).

Arthritis onset can be synchronized in SKG mice by injection of mannan(23). Male *Ptpn2*$^{+/-}$ SKG mice developed worse arthritis after injection of mannan,

correlating with significantly increased expression of the inflammatory cytokines *Il1b*, *Tnf*, *Il6*, *Tnfsf11 (*the gene encoding for RANK-ligand*)* and *Il17a* in arthritic ankles (Figure 2A-D). We also observed an increased severity of mannan-induced arthritis in female *Ptpn2*$^{+/-}$ SKG mice (data not shown). We conclude that *Ptpn2* haploinsufficiency, which reduces the expression of *Ptpn2* to levels comparable to what reported for carrier of disease associated *PTPN2* SNPs (Supplemental Figure 1F), enhances severity of arthritis in a T cell- but not in innate immune cell-mediated models of arthritis.

***Ptpn2* haploinsufficiency promotes enrichment of Th17 cells and ectopic lymphoid-like structures**

Next, we immunophenotyped *Ptpn2*$^{+/+}$ *and Ptpn2*$^{+/-}$ SKG mice subjected to mannan-induced arthritis. We found no difference in the number of total CD4 T cells or in effector populations Th1 and Th17 or Tregs in popliteal lymph nodes of *Ptpn2*$^{+/+}$ vs *Ptpn2*$^{+/-}$ SKG mice (Figure 3A).

In SKG arthritic ankles we mainly found CD4 T cells with an effector phenotype (Figure 3B) while, consistent with previous reports, CD8 T cells were almost absent (24, 25). Arthritic joints from *Ptpn2*$^{+/-}$ SKG mice displayed increased numbers CD4 T cells with specific expansion of Th17 cells when compared to *Ptpn2*$^{+/+}$ SKG mice (Figure 3C-E). There was no difference in the number of either RORγt^{+} or RORγt^{-} Tregs, and no Th1 cells were found within arthritic ankles (Figure 3D, E). There was a significant correlation between the number of Th17 cells in arthritic ankles and the clinical arthritis score (Figure 3E), suggesting that the arthritogenic action of *Ptpn2* haploinsufficiency in SKG mice is mediated through increased joint accumulation of Th17 cells.

Assessment of synovial tissue from arthritic *Ptpn2*$^{+/-}$ SKG mice also displayed an increased presence of lymphoid nodules composed by B cells (B220+), clustering within close proximity to CD4 T cell (Figure 3F, G). The formation of these lymphoid nodules was reminiscent of the ectopic lymphoid structures (ELS) that are present within the synovium of a subgroup of RA patients and correlate with more severe disease course(26). Th17 cells can contribute to the formation of ELS through production of IL-17 which stimulates expression of

CXCL13(26, 27). Consistent with the increased accumulation of Th17 cells in *Ptpn2*$^{+/-}$ SKG arthritic ankles, we found an increased expression of ELS-associated genes including *Cxcl12, Cxcl13*, *Lta*, *Ltb* and *Prdm1*(28) in the same joints (Figure 3H), while there was no difference in the expression of *Bcl6*. Together, these results further support the notion that increased arthritis in *Ptpn2*$^{+/-}$ SKG mice is mediated through a Th17-dependent mechanism.

T cell specific haploinsufficiency of *Ptpn2* promotes arthritis

Previous studies have concluded that B cells play a minor role, if any, in SKG arthritis(24). Accordingly, B cell depletion during the arthritic phase did not influence disease severity in SKG mice (Supplemental Figure 2), thus it is unlikely that promotion of SKG arthritis by *Ptpn2* haploinsufficiency is mediated through an action on B cells.

We therefore turned our attention to T cells. To verify that the partial loss of function of *Ptpn2* promotes SKG arthritis through a T cell intrinsic mechanism, we generated SKG mice carrying T cell specific haploinsufficiency of *Ptpn2* on the B6 background. First, we backcrossed the SKG mutation onto the B6 background for 10 generations. Next, we made our B6.SKG mice congenic for the H2^{d} haplotype, thus generating B6.SKG.H2$^{d/d}$ mice. We verified that B6.SKG.H2$^{d/d}$ mice developed similar arthritis as SKG mice after injection of mannan, and displayed similar synovial inflammation and bone destruction (Figure 4A, B). Also, B6.SKG.H2$^{d/d}$ mice showed similar enrichment of Th17 cells in popliteal lymph nodes and arthritic ankles as seen in SKG mice (Figure 4C).

B6.SKG.H2$^{d/d}$ mice were further crossed with *Ptpn2* floxed (*Ptpn2*$^{fl/fl}$) and Lck-cre^{+} mice, thus generating B6.SKG.H2$^{d/d}$.*Ptpn2*$^{fl/+}$.Lck-cre^{+} mice carrying T cell specific haploinsufficiency of *Ptpn2* (Figure 4D). When subjected to mannan-induced arthritis, female and male B6.SKG.H2$^{d/d}$.*Ptpn2*$^{fl/+}$.Lck-cre^{+} mice displayed more severe disease compared to control B6.SKG.H2$^{d/d}$.*Ptpn2*$^{fl/+}$.Lck-cre^{-} mice (Figure 4E, F). We conclude that *Ptpn2* haploinsufficiency promotes development of SKG arthritis through an intrinsic effect on T cells.

***Ptpn2* haploinsufficient CD4 T cells transfer enhanced arthritis severity**

SKG CD4 T cells can transfer arthritis to Rag2-KO mice(23). As shown in Figure 5A-C, Rag2-KO transferred with CD4 T cells isolated from *Ptpn2*$^{+/-}$ SKG mice developed significantly worse arthritis than mice transferred with CD4 T cells from *Ptpn2*$^{+/+}$ SKG mice. Importantly, transfer of *Ptpn2*$^{+/-}$ SKG CD4 T cells also caused increased formation of lymphoid nodules in arthritic ankles of Rag2-KO mice (Figure 5D). These data confirm that *Ptpn2* haploinsufficiency enhances arthritis through an action on CD4 T cells.

In order to understand how *Ptpn2* haploinsufficiency affects CD4 T cell differentiation during SKG arthritis, we generated CD4 T cell chimeras by transferring CD4 T cells isolated from pre-arthritic CD45.1 and CD45.2 *Ptpn2*$^{+/+}$ or *Ptpn2*$^{+/-}$ SKG mice into Rag2-KO mice (Figure 5E). Assessment of arthritic chimeric mice revealed preferential expansion of *Ptpn2*$^{+/-}$ SKG CD4 T cells over *Ptpn2*$^{+/+}$ SKG CD4 T cells in lymph nodes (Figure 5F). We observed preferential expansion of *Ptpn2*$^{+/-}$ SKG Treg in the spleen and of Th1 and especially Th17 cells in lymph nodes (Figure 5G, H). The above-mentioned phenotype was not due to differences in the frequencies of naïve or effector subsets of CD4 T cells in the pre-arthritic mice used for adoptive transfer (Supplemental Figure 3A). We conclude that *Ptpn2* haploinsufficiency leads to increased expansion of SKG CD4 T cells and their effector subsets after transfer into lymphopenic hosts.

Thymic selection and TCR signaling are not altered by *Ptpn2* haploinsufficiency

Complete deletion of *Ptpn2* in T cells alters thymic selection and promotes peripheral expansion of specific T cell clones, effects depending on the role of PTPN2 as a negative regulator of TCR signaling (9, 10, 29). However, we did not find any evidence for altered thymic selection or selective expansion of specific peripheral Vβ CD4 T cell clones in *Ptpn2*$^{+/-}$ SKG mice compared to *Ptpn2*$^{+/+}$ SKG mice (Supplemental Figure 3B, C). Also, we did not detect any differences in the induction of CD69 or CD25 after TCR stimulation between *Ptpn2*$^{+/+}$ and *Ptpn2*$^{+/-}$ naïve SKG CD4 T cells (Supplemental Figure 4A, B). Although further studies are needed to conclusively rule out a role for a *Ptpn2* haploinsufficiency in thymic selection, our data strongly suggest that *Ptpn2* haploinsufficiency promotes

arthritis development through peripheral expansion of pathogenic Th17 and perhaps also Th1 cells.

Increased sensitivity to IL-2 in *Ptpn2* haploinsufficient CD4 T cells

Although an expansion of *Ptpn2*$^{+/-}$ Th1 cells was only observed T cell chimeric mice and not in arthritic *Ptpn2*$^{+/-}$ SKG mice, we did consider a potential arthritogenic role of *Ptpn2* haploinsufficient Th1 cells. Since IL-2 promotes differentiation of Th1 cells(30) and previous reports have identified PTPN2 as an important negative regulator of IL-2 signaling in CD4 T cells(9), we first assessed IL-2-signaling in pre-activated *Ptpn2*$^{+/+}$ vs. *Ptpn2*$^{+/-}$ naïve SKG CD4 T cells. In line with previous reports, we found increased IL-2 induced activation of STAT5 in naïve *Ptpn2*$^{+/-}$ SKG CD4 T cells (Supplemental Figure 4C). This enhanced sensitivity to IL-2 correlated with significantly increased differentiation into Th1 cells from naïve *Ptpn2*$^{+/-}$ SKG CD4 T cells while there was no evidence of enhanced IFNγ signaling (Supplemental Figure 4D, E). However, IFNγ-producing SKG CD4 T cells -i.e. Th1 cells- play a protective role in SKG arthritis(31). Accordingly, global KO of IFNγ aggravated arthritis development in SKG mice (Supplemental Figure 4F). We conclude that although increased IL-2 signaling in *Ptpn2*$^{+/-}$ SKG mice can promote Th1 (and potentially Treg) expansion, Th1 cells are unlikely to mediate the increased arthritis severity observed in these mice.

Enhanced arthritis is driven by IL-6 and IL-17

Development of arthritis in SKG mice is partially dependent on IL-6 and IL-17(23, 25, 31). We verified the IL-17-dependence of SKG arthritis and lymphoid nodule development by treating SKG and SKG CD4 T cell-recipient Rag2-KO mice with IL-17A-neutralizing antibodies during the course of mannan-induced arthritis (Supplemental Figure 5A-D). To determine if enhanced arthritis in *Ptpn2*$^{+/-}$ SKG mice was IL-17- and/or IL-6 dependent, we treated *Ptpn2*$^{+/+}$ and *Ptpn2*$^{+/-}$ SKG mice with IL-17A-neutralizing or IL-6-receptor (IL6-R)-blocking antibodies. Both treatments eliminated differences in arthritis development and lymphocyte accumulation in arthritic ankles between *Ptpn2*$^{+/+}$ and *Ptpn2*$^{+/-}$ SKG mice (Figure 6A-C), while only partially suppressing disease development. Another cytokine that is important for the pathogenesis of arthritis in SKG mice is TNFα(25).

However, we did not find any difference in TNFα production between *Ptpn2*$^{+/+}$ and *Ptpn2*$^{+/-}$ SKG CD4 T cells (Supplemental Figure 5E). These data suggest that the increased arthritis in *Ptpn2*$^{+/-}$ SKG mice is driven by IL-6 and IL-17 but not by increased TNFα production from CD4 T cells. We only detected minimal IL-6 production from SKG CD4 T cells which was unaffected by *Ptpn2* haploinsufficieny (Supplemental Figure 5F, G) pointing to T cell extrinsic sources of IL-6 as critical for the enhanced arthritis of *Ptpn2*$^{+/-}$ SKG mice.

PTPN2 haploinsufficiency promotes conversion of Tregs

IL-6 is required for the differentiation of naïve CD4 T cells into Th17(32). In contrast to previous reports showing that complete loss of *Ptpn2* promotes Th17 differentiation(13), naïve SKG CD4 T cells from *Ptpn2*$^{+/-}$ mice did not display enhanced capacity for Th17 differentiation in vitro (Figure 6D). This was not due to an altered expression of the *il6ra* complex in *Ptpn2*$^{+/-}$ naïve SKG CD4 T cells (Supplemental Figure 5H). Thus, the accumulation of Th17 observed in arthritic joints of *Ptpn2*$^{+/-}$ SKG mice is unlikely due to increased differentiation of naïve CD4 T cells into Th17.

IL-6 dependent conversion of FoxP3^{+} Tregs into IL-17-producing FoxP3^{-} T cells has previously been reported in the collagen induced arthritis (CIA) model, and suggested as a source of autoreactive IL-17 producing cells in RA(33). We therefore questioned whether *Ptpn2* haploinsufficiency promotes IL-6-dependent loss of Foxp3 by Treg and trans-differentiation into IL-17-producing T cells in SKG mice. Figure 6E show that *Ptpn2*$^{+/-}$ SKG Tregs displayed enhanced IL-6-induced in vitro conversion into IL-17 producing Foxp3^{-} cells. Similar to naïve SKG CD4 T cells, *Ptpn2*$^{+/-}$ SKG Tregs did not show any change in *Il6r* expression (Supplemental Figure 5H). Next, we assessed the stability of SKG Tregs during arthritis in vivo by co-transferring CD45.2 SKG CD4 FoxP3^{+} Tregs with CD45.1 SKG CD4^{+} CD25^{-} T cells to Rag2-KO mice and subjecting recipient mice to mannan-induced arthritis (Supplemental Figure 5I, J). We found that during arthritis, *Ptpn2* haploinsufficient Tregs displayed significantly increased conversion into Foxp3^{-} IL-17A-producing cells (exTregs, Figure 6F). These data point to a role of PTPN2 as a regulator of Treg stability during autoimmune inflammation.

Treg-specific *Ptpn2* haploinsufficiency promotes SKG arthritis

To further assess how *Ptpn2* haploinsufficiency influences Treg function during arthritis we generated a Treg fate mapping SKG mouse model by crossing B6.SKG.H2$^{d/d}$.FoxP3$^{YFP\text{-}cre}$ mice with B6.SKG.H2$^{d/d}$.ROSA-26-tdTomato reporter mice and B6.SKG.H2$^{d/d}$.*Ptpn2*$^{fl/+}$ mice. The resulting mice (B6.SKG.H2$^{d/d}$.FoxP3$^{YFP\text{-}cre+/-}$.tdTom$^{fl/+}$.*Ptpn2*$^{fl/+\ or\ +/+}$, Figure 7A) carry Treg-specific haploinsufficiency of *Ptpn2*, in which YFP identifies cells currently expressing FoxP3 (Tregs), whereas tdTomato marks cells that are expressing (Tregs) or did express FoxP3 (exTregs). When subjected to mannan-induced arthritis, we found that female mice carrying Treg-specific haploinsufficiency of *Ptpn2* displayed enhanced arthritis severity (Figure 7B). *Ptpn2* haploinsufficient Tregs did not display reduced suppressive functions (Supplemental Figure 6A, B), consistent with previous data from complete KO Tregs(9). Instead, increased arthritis in mice carrying Treg-specific *Ptpn2* haploinsufficiency correlated with increased frequencies of IL-17 producing exTregs in both joint draining lymph nodes and arthritic ankles (Figure 7C). Importantly, frequencies of Th17 (YFP$^-$IL17$^+$IFNγ^- tdTom$^-$ CD4 cells) in the lymph nodes and joints were unaffected by haploinsufficiency of *Ptpn2* in Treg (Figure 7D). Transfer of in vitro generated exTregs to Rag2-KO mice was sufficient to induce arthritis and transfer of *Ptpn2*$^{+/-}$ exTregs led to a faster onset and more severe arthritis compared to transfer of *Ptpn2*$^{+/+}$ exTregs (Figure 7E). We conclude that *Ptpn2* haploinsufficiency promotes arthritis at least in part at the Treg level, by rendering Tregs more susceptible to FoxP3 loss and conversion into IL-17-producing arthritogenic exTreg cells.

The expression profile of exTregs are distinct from Tregs

To further characterize IL-17$^+$ exTregs and their relationship to Tregs, we performed RNA-seq on exTregs and Tregs sorted from arthritic Treg fate mapping mice (Supplemental Figure 6C). We identified around 1820 differentially expressed genes (DEG, fold diff.>2, *Padj*<0.05) between Tregs and exTregs (Figure 8A). Several Th17-associated genes (e.g. *Il17a, Rorc, Il22, Il23r)* were found to be upregulated in exTregs whereas several Treg-associated genes (e.g. *Foxp3, Ctla4, Grzmb, Gpr83)* were downregulated in exTregs (Figure 8A). Gene-expression

clustering (fold diff.>2, *Padj*<0.05) confirmed highly differential transcriptional patterns between exTregs and Tregs indicating that exTregs represents a unique population which has lost its Treg identity (Figure 8B, C). IL-17^{+} exTregs also expressed several genes important for homing to synovial tissue and RA pathogenesis, e.g. *Cxcr6, Ccr6, Ccl20, Tnfsf11* (Figure 8A-C). Interestingly, a comparison of gene-expression between *Ptpn2*$^{fl/+}$ and *Ptpn2*$^{+/+}$ exTregs did not reveal any difference (Figure 8D), suggesting that PTPN2 is an upstream regulator of pathways that control Treg stability rather than skewing specific transcriptional patterns in exTregs.

In vitro generated exTregs recapitulate in vivo exTregs

We next sought to assess whether the exTregs generated in our in vitro conversion assay display sufficient similarities to the exTregs found in vivo to enable mechanistic studies of the role of PTPN2 in Treg stability. RNA-seq was performed on IL-17A^{+} exTregs and IL-17A^{-} Tregs isolated after 72h of in vitro conversion assay using Tregs from *Ptpn2*$^{+/+}$ and *Ptpn2*$^{+/-}$ FoxP3^{eGFP} SKG mice (Supplemental Figure 7A). Gene-expression clustering revealed separated genetic expression profiles between Tregs and in vitro generated exTregs (Figure 9A). We identified around 870 differentially DEG (DEG, fold diff.>2, *Padj*<0.05) between Tregs and in vitro generated exTregs (Supplemental Figure 7B). Although in vitro generation of exTreg resulted in a reduced number of DEG when compared to in vivo exTreg, in vitro generated exTreg showed highly similar enrichment in Th17 associated genes (e.g. *Il17*, *Rorc, and Tnfsf11)* and reduced expression of Treg-associated genes (e.g. *Foxp3* and *Ctla4)* (Figure 9A, B). When we compared the expression of 30 genes that have been reported to define the Th17 and Tregs transcriptional programs (15, 33-36), we found very high similarity between exTregs isolated from fate mapping mice, and in vitro generated exTreg (Figure 9C, Supplemental Figure 7C, D). The similarity in gene-expression profile between in vitro and in vivo exTregs was further supported by pathway analysis, which showed almost identical pathway enrichment between the two populations (Supplemental Figure 7E). Furthermore, as seen in vivo*,* there was no difference in gene-expression profiles between in vitro generated *Ptpn2*$^{+/+}$ and *Ptpn2*$^{+/-}$

exTregs (Supplemental Figure 7F). We conclude that in vitro IL-6-induced exTregs do display high phenotypic similarity to exTregs found in vivo in arthritic SKG mice. The residual difference between the transcriptomes of in vitro IL-6-induced and in vivo exTregs suggest that additional stimuli are needed to fully in vitro recapitulate either the population heterogeneity or the transcriptional program of in vivo exTregs.

exTregs display a unique chromatin landscape

Next, we assessed if generation of exTregs was also associated with changes in chromatin accessibility. SKG Tregs were stimulated with IL-6 in vitro and isolated after 24h (Treg 24h), 48h (Treg 48h) and 72h (Treg 72h) of culture and their chromatin accessibility profiles were compared to exTregs isolated after 72h of stimulation (exTregs 72h) using ATAC-Seq (Figure 10A and Supplemental Figure 7G). Comparison of exTregs 72h with Treg 24h identified more than 30,000 differentially accessible regions (Figure 10B), while comparison with Treg 48h identified over 21,000 differentially accessible regions and comparison with Tregs 72h showed around 15,000 differentially accessible regions (Figure 10C, D). Furthermore, comparison of differentially accessible regions between Tregs at different stages of dedifferentiation demonstrated that exTregs possess a unique set of regions with enhanced or suppressed accessibility, while Tregs 48h displayed an expanded set of regions with enhanced accessibility when compared to Tregs at other time points (Figure 10E-F).

Compared to Tregs, exTregs showed an almost complete lack of accessible chromatin pattern at the *Foxp3* loci, which was similar to that seen in sorted Th17 cells (Figure 10H). Evaluation of the *Rorc* loci showed gradually increasing chromatin accessibility during Treg dedifferentiation and Tregs and exTregs after 72h displayed a pattern similar to that seen in Th17 cells (Figure 10I). However, in contrast to the *Rorc* loci, only exTregs showed a pattern of increased chromatin accessibility similar to Th17 cells in the extended *Il17a* and *Il17f* loci (Figure 10J).

Together these results suggest that during IL-6 driven dedifferentiation, Tregs undergo specific changes in chromatin accessibility which include a progressive opening of the *Rorc* loci. On the other hand, exTreg display a unique

chromatin landscape compared to Tregs at other stages, characterized, among other changes, by the closure of the *FoxP3* loci and increased chromatin accessibility of the *Il17* loci, conducive to active *Il17* transcription. Furthermore, the concentration of newly opened loci at 48h of stimulation suggest that key molecular mechanisms of Treg destabilization occur at this stage.

***Ptpn2* regulates stability of RORγt$^+$ effector Tregs**

Consistent with the above-mentioned chromatin accessibility assessment, analysis of in vitro SKG exTreg generation showed that IL-6-driven conversion into FoxP3$^-$ exTregs occurs via upregulation of RORγt in Tregs followed by subsequent loss of FoxP3 from RORγt$^+$ Tregs and expression of IL-17 in RORγt$^+$FoxP3$^-$ exTregs (Figure 11A). RORγt$^+$ Tregs have been described in vivo as having an effector phenotype(37, 38). In line with previous reports, RORγt$^+$ SKG Tregs displayed an effector phenotype with high expression of CD44 and low expression of CD62L and also showed high expression of ICOS and CCR6 similar to Th17 cells (Supplemental Figure 8A).

Next, we sorted effector and resting Tregs from *Ptpn2*$^{+/+}$ and *Ptpn2*$^{+/-}$ FoxP3^{eGFP} SKG mice and subjected them to in vitro conversion (Supplemental Figure 8B). We further confirmed that *Rorc* was primarily expressed in effector Tregs by qPCR and flow cytometry (Supplemental Figure 8B-D, expression of *Prdm1* was used to confirm sorting of effector Tregs). There was no difference in expression of *Foxp3* between sorted effector and resting Tregs (Supplemental Figure 8C), however effector Tregs showed enhanced tendency to lose FoxP3 and convert into IL-17$^+$ exTregs despite lower expression of IL-6 receptors (Figure 11B-D and Supplemental Figure 8E). As shown in Figure 11B-D, *Ptpn2* haploinsufficiency (which resulted in 50% reduction of *Ptpn2* expression, Supplemental Figure 8F) selectively enhanced the in vitro conversion of effector but not resting Tregs into exTregs. This was not associated with decreased expression of CD25 in effector Tregs -which reportedly correlates with enhanced Treg to exTreg conversion(33)- or with differences in expression of RORγt between *Ptpn2*$^{+/+}$ and *Ptpn2*$^{+/-}$ resting or effector Tregs (Supplemental Figure 8A, G, H). These data suggest that IL-17-producing exTregs are generated via loss of FoxP3

by effector RORyt$^+$ Tregs and that *Ptpn2* selectively promotes FoxP3 stability in effector RORyt$^+$ Tregs but not IL-6 induced induction of RORγt in Tregs.

Ptpn2 haploinsufficiency promotes IL-6 induced FoxP3 instability in effector RORγt$^+$ Tregs

To further evaluate the mechanism by which IL-6 promotes conversion of Treg into exTreg, we treated *Ptpn2*$^{+/+}$ and *Ptpn2*$^{+/-}$ resting Tregs, which have low or no expression of RORγt, with Ruxolitinib, an inhibitor of the JAK1-2/STAT3 pathway downstream the IL-6 receptor(39, 40). Ruxolitinib significantly reduced IL-6- induced loss of FoxP3 from RORγt$^+$ Tregs and the generation of IL-17$^+$ exTregs and obliterated the effect of *Ptpn2* haploinsufficiency on the conversion of RORγt$^+$ Tregs into IL-17$^+$ exTregs without affecting Treg survival within the time-frame of the assay (Figure 11E, F and Supplemental Figure 8I). However, neither Ruxolitinib nor *Ptpn2* haploinsufficiency affected IL-6-induced upregulation of RORγt in resting Tregs (Figure 11E, F). These data provides evidence that Treg to exTreg conversion is promoted by IL-6-induced activation of the JAK/STAT pathway, although further studies in vivo – e.g. via Ruxolitinib treatment - are warranted to solidify the role of this pathway for in vivo exTreg generation. Interestingly, inhibition of RORγt function did not block IL-6-induced loss of FoxP3 by RORγt$^+$ Tregs, despite suppressing expression of IL-17 from exTregs (Supplemental Figure 8J, K).

PTPN2 regulates FoxP3 stability in effector Tregs through binding and dephosphorylation of STAT3

In order to identify potential molecular mechanisms of action of PTPN2 we interrogated the above-mentioned chromatin landscape data looking for transcription factor (TF) binding motifs that are differentially accessible at consecutive stages of IL-6 induced Treg dedifferentiation. We found that in the first 48h there was an enrichment of motifs for TF belonging to the bZIP family whereas accessibility of binding motifs for the ETS-family TF was reduced. After an additional 24h the same trend toward increased accessibility for bZIP-family TF and decreased accessibility for ETS-family TF was observed in converted exTregs 72h, which in addition also displayed enrichment of motifs for Runt-family TF. On

the contrary, non-converted Tregs 72h displayed an opposite profile characterized by enrichment of ETS-family TF motifs and reduction in bZIP-family TF motifs (Figure 12A). Several members of the bZIP transcription factor family (such as BATF, JunB and Fosl2) have been associated with the Th17 differentiation program(35, 41), whereas members of the ETS family (such as ETS-1) have been associated with stabilization and functions of Tregs(42, 43). Among members of the Runt TF family, Runx1 has an important role in promoting IL-17 production through direct interaction with RORγt(44).

At no stage of Treg dedifferentiation could we observe differences in chromatin accessibility between *Ptpn2*$^{+/+}$ and *Ptpn2*$^{+/-}$ (Supplemental Figure 8L), suggesting that PTPN2 does not affect Treg dedifferentiation by skewing chromatin accessibility to the above-mentioned TF. However, although we did not find enrichment of STAT3 binding motifs (but we cannot rule out effects before the time points considered in this study), we noticed that several TF (indicated by arrows in Figure 12A) that bind to motifs displaying enhanced accessibility in Treg 48h (the stage at which conversion process is maximized) and in exTregs 72h are known in CD4 T cells to mediate functions of STAT3(35, 45).

Since STAT3 is a known substrate for PTPN2, we hypothesized that *Ptpn2* haploinsufficiency promotes Treg instability via abnormal regulation of STAT3 phosphorylation in RORγt^{+} effector Treg. Consistent with our hypothesis, we observed an enhanced activation of STAT3 in effector *Ptpn2*$^{+/-}$ SKG Tregs after IL-6 stimulation when compared to *Ptpn2*$^{+/+}$ SKG Tregs (Figure 12B). To confirm that PTPN2 regulates Treg conversion through an action on STAT3 we sorted Tregs from *Ptpn2*$^{fl/fl}$ (PTPN2-WT), Lck-Cre.*Ptpn2*$^{fl/fl}$ (PTPN2-KO) and Lck-Cre.*Ptpn2*$^{fl/fl}$.*Stat3*$^{fl/+}$ (PTPN2-KO, STAT3-het) WT mice. PTPN2-KO Tregs showed enhanced susceptibility to conversion into exTregs, which was abrogated by semi-loss of STAT3 (Figure 12C and Supplementary Figure 8M).

In further support that STAT3 is a target for PTPN2 in Treg, we could co-immunoprecipitate PTPN2 and STAT3 from lysates of in vitro expanded Tregs (Figure 13A). To confirm a direct functional interaction between PTPN2 and STAT3 we performed in vitro dephosphorylation and substrate trapping experiments. In

support of a direct role of PTPN2 in regulation of STAT3 activation, we found that PTPN2 dephosphorylates STAT3 pY705 (Figure 13B). Furthermore, we found that a substrate trapping mutant of PTPN2 (D182A, Q260A) could form a physical complex with phosphorylated STAT3 (pTyr705) but not with unphosphorylated STAT3 (Figure 13C).

Together, these results suggest a model (Figure 13D) where PTPN2 selectively inhibits JAK/STAT-dependent loss of FoxP3 in IL-6-stimulated RORγt^{+} effector Treg- at a stage when chromatin accessibility for Treg destabilizing TF is maximized- which in turn inhibits RORγt-dependent IL-17 production. IL-6-induced upregulation of RORγt in Treg does not promote loss of FoxP3 and surprisingly appears to occur through a JAK- and PTPN2-independent pathway.

Discussion

In this study we aimed to clarify the functional genetics of *PTPN2* in autoimmunity by focusing on mouse models of RA carrying semi-deletion of *Ptpn2* which reduces the expression of *Ptpn2* in immune cells to a level comparable to what has been reported in human carriers of RA- and IBD-associated *PTPN2* haplotypes. Global deletion of *Ptpn2* in BALB/c mice results in spontaneous subchondral bone erosion and synovitis, however no further experimental investigation of the role of PTPN2 in RA has been reported(46). Although *Ptpn2* haploinsufficiency does not trigger spontaneous autoimmunity in B6 mice(9), we show that it is able to enhance incidence and severity of disease on an autoimmune-prone background. This exemplifies the importance of modeling human autoimmune-associated variants in an autoimmunity-prone context, reflecting the additional risk factors that are needed in humans to trigger disease.

Our data points to haploinsufficiency of *Ptpn2* being able to sustain some but not all of the immunological functions reported for *Ptpn2*(9-11, 29). For example, while complete deletion or deep knockdown of *Ptpn2* revealed a major role of this enzyme in limiting myeloid cell and synoviocyte-driven inflammation(7, 18), we find that innate immune cells are not critical mediators of the pathogenic action of *Ptpn2* haploinsufficiency. We show here that *Ptpn2* haploinsufficiency in autoreactive T cells promotes expansion of Th1, Treg and pathogenic Th17 cells under lymphopenic conditions. Complete deletion of *Ptpn2* is known to promote lymphopenic expansion of naive CD4 and CD8 T cells through enhancement of TCR signaling, while IL-7 signaling was unaffected(29). However, we did not find significant evidence of increased TCR signaling in *Ptpn2* haploinsufficient SKG mice. Similarly, conditional haploinsufficiency of *Ptpn2* in T cells on the B6 background did not result in increased TCR sensitivity or altered thymic selection(9). On the other hand, the enhanced IL-2 signaling found in *Ptpn2* haploinsufficient T cells is reminiscent of the phenotype of *Ptpn2*$^{-/-}$ T cells which display increased IL-2 mediated Treg expansion(9, 47). Thus, we speculate that enhanced IL-2 signaling underlies the observed expansion of *Ptpn2* haploinsufficient Th1 and Tregs in lymphopenic conditions. *Ptpn2*

haploinsufficiency also led to marked expansion of pathogenic IL-17 producing CD4 T cells after transfer of SKG CD4 T cells into lymphopenic hosts. However, in contrast to previous reports on naïve *Ptpn2*$^{-/-}$ T cells, *Ptpn2* haploinsufficient naïve CD4 T cells did not show increased IL-6-driven differentiation into Th17. This could be due to differences between WT and SKG naïve T cells or between IL-6 vs IL-2 signaling amplification is *Ptpn2*$^{-/-}$ vs *Ptpn2*$^{+/-}$ T cells.

Here we suggest that loss of FoxP3 by RORγt^{+} Treg significantly contributes to the increased numbers of IL-17-producing cells observed in *Ptpn2*$^{+/-}$ arthritic mice. We show that Treg-specific haploinsufficiency of *Ptpn2* is sufficient to enhance severity of arthritis in SKG mice and replicates the phenotype seen in mice carrying haploinsufficiency of *Ptpn2* in all T cells. We did not find any defect of suppressive function of *Ptpn2* haploinsufficient Tregs, consistent with previous data in mice carrying complete deletion of *Ptpn2*(9). However, *Ptpn2* haploinsufficient RORγt^{+} Tregs are more sensitive to IL-6-dependent loss of FoxP3 and conversion into IL-17A-producing exTregs that can transfer arthritis to Rag2-KO recipient mice. Since no conditional deletion of *Ptpn2* or of other tyrosine phosphatases in Tregs has been reported to date and the role of *Ptpn2* in Treg in the context of inflammation has not been explored yet, our results also highlight for the first time a potential role of a tyrosine phosphatase in Treg stability in the context of autoimmune inflammation.

Since it has been reported that complete loss of *Ptpn2* causes expansion of Treg and enhances FoxP3 stability in inducible Tregs(9, 16), we were surprised to find that *Ptpn2* haploinsufficiency promotes autoimmunity through destabilization of Treg. Also the enhanced in vitro IL-2 signaling observed in *Ptpn2* haploinsufficient naïve CD4 T cells and the potentially IL-2 signaling dependent expansion of disease-protective Th1 and Treg in lymphopenic animals might sound inconsistent with the proposed arthritogenic role of *Ptpn2* haploinsufficiency in SKG mice. However, in arthritic *Ptpn2*$^{+/-}$ SKG mice we could not detect any expansion of Th1 or Treg. Thus, in non lymphopenic conditions, the IL-2 signaling enhancing effect of *Ptpn2* haploinsufficiency might be limited and/or its disease

protective effect neutralized by enhanced IL-6 signaling, which also might offset any potential Treg expansion via Treg destabilization.

Our data lend support to previous observations that loss of FoxP3 in Tregs is responsible for generation of pathogenic T cells during autoimmune diabetes(48) and in CIA(33). However, the molecular mechanism of FoxP3 loss in Treg has remained unexplored. Here we show that during IL-6 driven dedifferentiation, Tregs undergo specific changes in chromatin accessibility. In this context, enhanced IL-6-dependent loss of FoxP3 in *Ptpn2* haploinsufficient Treg correlates with enhanced phosphorylation of STAT3, and depends on JAK activity and STAT3 expression. Importantly, T cell phenotyping and chromatin analysis shows that loss of *Ptpn2* selectively destabilizes effector Treg and suggests that STAT3 phosphorylation in Treg is only able to modulate FoxP3 stability in RORγt$^+$ Treg, without affecting IL-6-dependent RORγt expression. Thus, our data also suggest potential differences in signaling pathways mediating IL-6 dependent RORγt induction and in downstream STAT3-dependent signaling between Treg and FoxP3-negative T cells.

In conclusion, reduced *Ptpn2* expression promotes arthritis through enhanced IL-6 signaling in effector Tregs, causing increased STAT3 phosphorylation that renders RORγt$^+$ Tregs more susceptible to loss of FoxP3. It remains to be established whether the arthritogenic effect of *Ptpn2* haploinsufficiency is exerted on natural Treg and/or peripherally-induced Treg. Also, the importance of PTPN2 as a regulator of JAK/STAT signaling suggests that further studies on the potential role of *Ptpn2* haploinsufficiency in enhancing signaling of additional JAK/STAT activator cytokines that might play a role in the pathogenesis of SKG arthritis (e.g. IL-23 and IL-10) are warranted.

Our study shows the importance of considering gene dosage when performing functional genetics studies and sheds light on unexpected functions of tyrosine phosphatases and the potential uniqueness of signaling pathways involved in Treg stability. Further studies of tyrosine phosphatases in resting vs effector Treg and of the molecular program underlying STAT3-dependent loss of

FoxP3 in effector Treg hold the promise to unravel novel mechanisms of tolerance and autoimmunity.

Methods

Mice

SKG mice have already been described(23). *Ptpn2*$^{+/-}$ BALB/c mice has been previously described(12). Generation of *Ptpn2* floxed (*Ptpn2*$^{fl/fl}$) B6 mice has recently been described(49). B6 mice congenic for the H2^{d} haplotype (JAX # 000359, B6.C-*H2*^{d}/bByJ), B6 FoxP3$^{YFP\text{-}cre}$ (JAX# 016959, B6.129(Cg)-*Foxp3*$^{tm4(YFP/icre)Ayr}$/J(50)), B6 ROSA-26-tdTomato (JAX# 007914, B6;Cg-*Gt(ROSA)26Sor*$^{tm14(CAG\text{-}tdTomato)Hze}$/J (51)), BALB/c FoxP3-eGFP (JAX# 006769, C.Cg-*Foxp3*^{tm2Tch}/J (52)), BALB/c CD45.1 (JAX# 006584, CByJ.SJL(B6)-*Ptprc*^{a}/J) and BALB/c (JAX# 000651, BALB/cJ) mice were all obtained from Jackson Laboratories (JAX). BALB/c Rag2-KO mice were purchased from Taconic (model 601). Above mice were housed at the La Jolla Institute for Allergy and Immunology (LJI) and University of California, San Diego (UCSD) vivarium under specific pathogen free conditions (SPF). *Ptpn2*$^{fl/fl}$.Lck-Cre^{+} (C57BL/6)(9) and *Stat3*^{floxed} mice were housed at the Peter MacCallum Cancer Center (Melbourne, Australia).

Arthritis models

For the K/BxN serum transfer model, arthritis was induced in 8-week-old male BALB/c mice by intraperitoneal (i.p.) injection of serum obtained from arthritic K/BxN mice. Every 2 days, development of arthritis was assessed by measurement of ankle thickness using a digital caliper according to an established protocol(53).

For the SKG mouse model, both spontaneous and mannan-induced arthritis were assessed. For mannan-induced arthritis, male and female mice were injected i.p. with 20 mg of mannan (Sigma Aldrich), dissolved in sterile PBS at 8 weeks of age. Clinical scoring and measurement of ankle thickness using a digital caliper was performed twice weekly according to an established protocol(24). Briefly clinical signs of arthritis in front and hind paws were scored as follows: 0, no joint swelling; 0.1 per swollen finger joint (3 digits on front paw and 4 digits on hind paw); 0.5, mild swelling of wrist or ankle; 1.0, severe swelling of wrist or ankle. Scores for all finger joints of forepaws and hindpaws, wrists and ankles were combined for each mouse yielding a maximum score of 5.4, which was considered

the clinical endpoint. Mice reaching clinical endpoint scores were sacrificed according to ethical guidelines.

For neutralization of IL-17, female and male SKG mice or Rag2-KO mice were injected with 100 µg of anti-IL17 antibody (clone 17F3, BioXcell) both retro-orbital (r.o.) and i.p. 1-2h before injection of mannan, after which mice received anti-IL-17 antibody once weekly (100 µg) by i.p. injection. For neutralization of IL-6 signaling, male SKG mice received weekly i.p. injections of 200 µg anti-IL-6R (clone 15A7, BioXcell) antibody with the first injection performed 2h before injection of mannan. Antibody treated mice were compared to control untreated mice.

All arthritis studies were performed on littermate mice. For treatment experiments, mice with the same genotype were randomly selected for treatment with cytokine neutralizing or control. Clinical scoring of mice was performed in a blinded manner in which genotypes and treatments were blinded to the researcher during scoring.

CD4 T cell transfer and generation of T cell chimeras in Rag2-KO mice

$2x10^6$ CD4 T cells isolated from spleen and lymph nodes of 8-week-old male *Ptpn2*$^{+/+}$ and *Ptpn2*$^{+/-}$ SKG mice using the EasySep™ Mouse CD4 T Cell Enrichment Kit (Stem Cell Technologies), were transferred to 8-week-old male Rag2-KO BALB/c mice through r.o. injection. The purity of isolated cells was verified by flow cytometry and was typically 95-98% with no contaminating B cells or CD8 T cells. Spontaneous development of arthritis was evaluated by clinical scoring and ankle thickness as described above.

For CD4 T cell chimera experiments, CD4 T cells were isolated from spleen and lymph nodes of 8-week old male CD45.1 and CD45.2 *Ptpn2*$^{+/+}$ and *Ptpn2*$^{+/-}$ SKG using the EasySep™ Mouse CD4 T Cell Enrichment Kit (Stem Cell Technologies). $1x10^6$ CD4 T cells from CD45.1 and CD45.2 mice were pooled in a 1:1 ratio (total of $2x10^6$ CD4 T cells / mouse) and transferred into 8-week-old male Rag2-KO mice. To account for any differences between CD45.1 and CD45.2 SKG mice, *Ptpn2*$^{+/+}$ and *Ptpn2*$^{+/-}$ CD4 T cells were isolated from both CD45.1 and CD45.2 mice and co-transferred with the opposite genotype isolated from either CD45.1 or CD45.2 mice.

In vitro Treg conversion assay

In vitro conversion assay of FoxP3^{+} Tregs were performed using a protocol adopted from Komatsu *et al*(33*).* Total FoxP3^{eGFP+} SKG Tregs (Supplemental Figure 5I) or effector (CD44^{hi}CD62L^{-}) and resting (CD44^{low}CD62L^{+}) FoxP3^{eGFP+} Tregs (Supplemental Figure 8B) were flow sorted from *Ptpn2*$^{+/+}$ and *Ptpn2*$^{+/-}$ 8-10 week-old female FoxP3^{eGFP+} SKG mice. Sorted Tregs were stimulated with Dynabeads mouse anti-CD3/CD28 T cell activation beads (Invitrogen) with or without addition of IL-6 (Biolegend, 50 ng/mL) for 24-72 hours. At the end of stimulation cells were re-stimulated with PMA (20 ng/mL), ionomycin (1 μM) and Brefeldin A for 5h and analyzed for the expression of IL-17A, FoxP3 and RORγt using flow cytometry. Ruxolitinib (Selleck Chemical) was used for inhibition of JAK1/2 signaling and the inverse agonist GSK805 (EMD Millipore Calbiochem) was used for inhibition of RORγt function.

For conversion assay using *Ptpn2*$^{fl/fl}$.Lck-Cre^{+} (WT), *Ptpn2*$^{fl/fl}$.Lck-Cre^{+} (PTPN2-KO) *Ptpn2*$^{fl/fl}$*Stat3*$^{fl/+}$.Lck-Cre^{+} (PTPN2-KO STAT3-Het) B6 mice, CD4^{+}CD25^{+} T_{reg} cells were sorted by flow cytometry and stimulated with plate-bound anti-CD3 (10 μg/ml) and soluble anti-CD28 (5 μg/ml) for 72h in the presence of IL-6 (50 ng/ml). After 72h cells were stimulated in the presence of Ionomycin (1 μg/ml), PMA (20ng/ml) and BD Golgi-Plug™ (BD Biosciences) and analysed for the expression of IL-17A, RORγt and FoxP3 using flow cytometry.

Further information regarding antibodies used for flow cytometry staining can be found in Supplemental Material.

In vivo Treg stability assay and transfer of exTregs to Rag2-KO mice

Tregs (CD4^{+}FoxP3^{eGFP+}) were flow sorted from spleen and lymph nodes of 8-week-old female *Ptpn2*$^{+/+}$ or *Ptpn2*$^{+/-}$ CD45.2 FoxP3^{eGFP} SKG mice, whereas CD4^{+}CD25^{-} cells were sorted from *Ptpn2*$^{+/+}$ or *Ptpn2*$^{+/-}$ 8-week-old female CD45.1 SKG mice (Supplemental Figure 5I, J). CD45.2 Tregs (3x10^{5}) were transferred in combination with CD45.1 CD4^{+}CD25^{-} SKG T cells (1.3x10^{6}) to 8-week-old female Rag2-KO mice. One week after transfer mice were injected with 20 mg of mannan to boost induction of arthritis. Tregs were analyzed in lymph nodes of arthritis mice using flow cytometry.

For evaluation of the pathogenicity of exTregs, Tregs were sorted from female *Ptpn2*$^{+/+}$ or *Ptpn2*$^{+/-}$ CD45.2 FoxP3^{eGFP} SKG mice as above. Isolated Tregs were subjected to in vitro conversion as described above. After 72h, *Ptpn2*$^{+/+}$ or *Ptpn2*$^{+/-}$ FoxP3^{eGFP-} exTregs were sorted (Supplemental Figure 7G) and transferred to female Rag2-KO mice (1.5x10^5 cells/mouse). Arthritis was induced 4 days after transfer by an i.p. injection with 20 mg of mannan. Mice were monitored for development of arthritis as described above.

Isolation of IL-17$^+$ exTregs and Tregs for RNA-sequencing

Isolation of in vivo IL-17$^+$ exTregs from B6.SKG.H2$^{d/d}$.FoxP3$^{YFP\text{-}cre+/-}$.tdTom$^{fl/+}$.*Ptpn2*$^{fl/+\ or\ +/+}$ was achieved by utilizing a mouse IL-17 Secretion assay kit (Miltenyl Biotec Inc. 130-094-207) according to manufactures protocol. Briefly, a single cell suspension was prepared from spleen and lymph nodes of female B6.SKG.H2$^{d/d}$.FoxP3$^{YFP\text{-}cre+/-}$.tdTom$^{fl/+}$.*Ptpn2*$^{fl/+}$ or B6.SKG.H2$^{d/d}$.FoxP3$^{YFP\text{-}cre+/-}$.tdTom$^{fl/+}$.*Ptpn2*$^{+/+}$ arthritic mice (50-70 days after mannan). Cells were stimulated with PMA (10 ng/mL) and ionomycin (1 ug/mL) in TexMACS media (Milteny Biotec) containing 5% mouse serum for 3h, after which cells were stained with a streptavidin labeled IL-17 capture reagent and incubated for 45 minutes. Cells were counterstained with anti-Biotin-APC, CD4, TCRβ, CD8, CD19 and fixable viability dye. IL-17$^+$ exTregs (Live cells CD8$^-$CD19$^-$TCRβ$^+$CD4$^+$tdTom$^+$YFP$^-$ IL17A$^+$) and IL-17$^-$ Tregs (Live cells CD8$^-$CD19$^-$TCRβ$^+$CD4$^+$tdTom$^+$YFP$^+$IL17A$^-$) were flow sorted directly into Trizol LS (Supplemental Figure 6C).

For isolation of in vitro generated IL-17$^+$ exTregs, Tregs (CD8$^-$CD19$^-$ CD4$^+$FoxP3^{eGFP+}) were sorted from female *Ptpn2*$^{+/+}$ or *Ptpn2*$^{+/-}$ FoxP3^{eGFP} SKG mice. Isolated Tregs were subjected to in vitro conversion as described above. IL-17$^+$ exTregs and IL-17$^-$ Tregs were isolated (Supplemental Figure 7A) using the IL-17 Secretion kit as described above.

Isolation of cells for ATAC-Sequencing

Th17 cells (Live CD8$^-$CD19$^-$CD4$^+$FoxP3^{eGFP-}CCR6^{hi}) and Tregs (Live CD8$^-$ CD19$^-$CD4$^+$FoxP3^{eGFP+}) were flow sorted from *Ptpn2*$^{+/+}$ *and Ptpn2*$^{+/-}$ female FoxP3^{eGFP} SKG mice (Supplemental Figure 7G). 1x10^5 Th17 and Tregs were directly prepared for ATAC-sequencing (described in supplemental methods).

Remaining Tregs were subjected to in vitro conversion as describe above. FoxP3^{eGFP+} (Tregs) cells were flow sorted after 24h, 48h and 72h of culture. FoxP3^{eGFP-} (exTregs) were sorted after 72h or culture (Supplemental Figure 7G).

Additional information regarding experimental methods can be found in Supplemental Methods.

Data availability

RNA-seq and ATAC-seq data discussed in this publication have been deposited in NCBI's Gene Expression Omnibus (GEO) and are accessible through GEO Series accession number GSE123488.

Statistics

Sample sizes were selected based upon our experience with the above-mentioned assays in order to achieve sufficient power to detect biologically relevant differences in the experiments being conducted with an α error (two tailed) <0.05.

For statistical analysis 2-tailed Mann-Whitney *U* test was performed on non-parametric data. On normally distributed data 2-tailed paired t-test or 2-tailed unpaired t-test were performed as reported in the figure legends. For comparison of multiple parameters 2-way ANOVA was used. All statistical analyses were performed using GraphPad Prism software. A comparison was considered significant if *P* was less than 0.05.

Study approval

The studies in animals were conducted in accordance with protocols approved by the Institutional Animal Care and Use Committee of LJI (protocol #AP140-NB4), the Institutional Animal Care and Use Committee of UCSD (protocol # S16098) and the NHMRC Australian Code of Practice for the Care and Use of Animals under approval of the Peter MacCallum Animal Ethics and Experimentation Committee (Ethics number: AEEC 570, 604).

Author Contributions

M.N.D.S. and N.B. conceived of, designed, and supervised the research, analyzed data and wrote the paper. M.N.D.S., K.M.D., B.J.S., D.J.W., C.S., W.B.K., B.P.,

S.B., F.W., R.G., G.S., E.S and S.Y., contributed to acquisition and analysis of data. I.A., G.K., P.M., S.S., M.K., M.L.T., P.V., T.T., F.A. provided tools and/or reagents and key scientific input. All authors approved the final version of the paper.

Acknowledgements

This study was funded in part by the Rheumatology Research Foundation (to N.B.), by the National Institutes of Health (NIH) Grants R01 AI070544 and AR066053 (to N.B.), P01 AI089624 (to M.K.) and S10OD016262 and S10RR027366 (to the La Jolla Institute), by Broegelmann Foundation (to P.M.) and Narodowe Centrum Nauki (NCN) (2014/14/E/NZ6/00162 to P.M.). K.M.D. was supported by a Canadian Institutes of Health Research Fellowship. D.J.W. was supported by NIH Training Grant T32 AR064194. T.T. is supported by the National Health and Medical Research Council of Australia (1103037).

Figures and legends

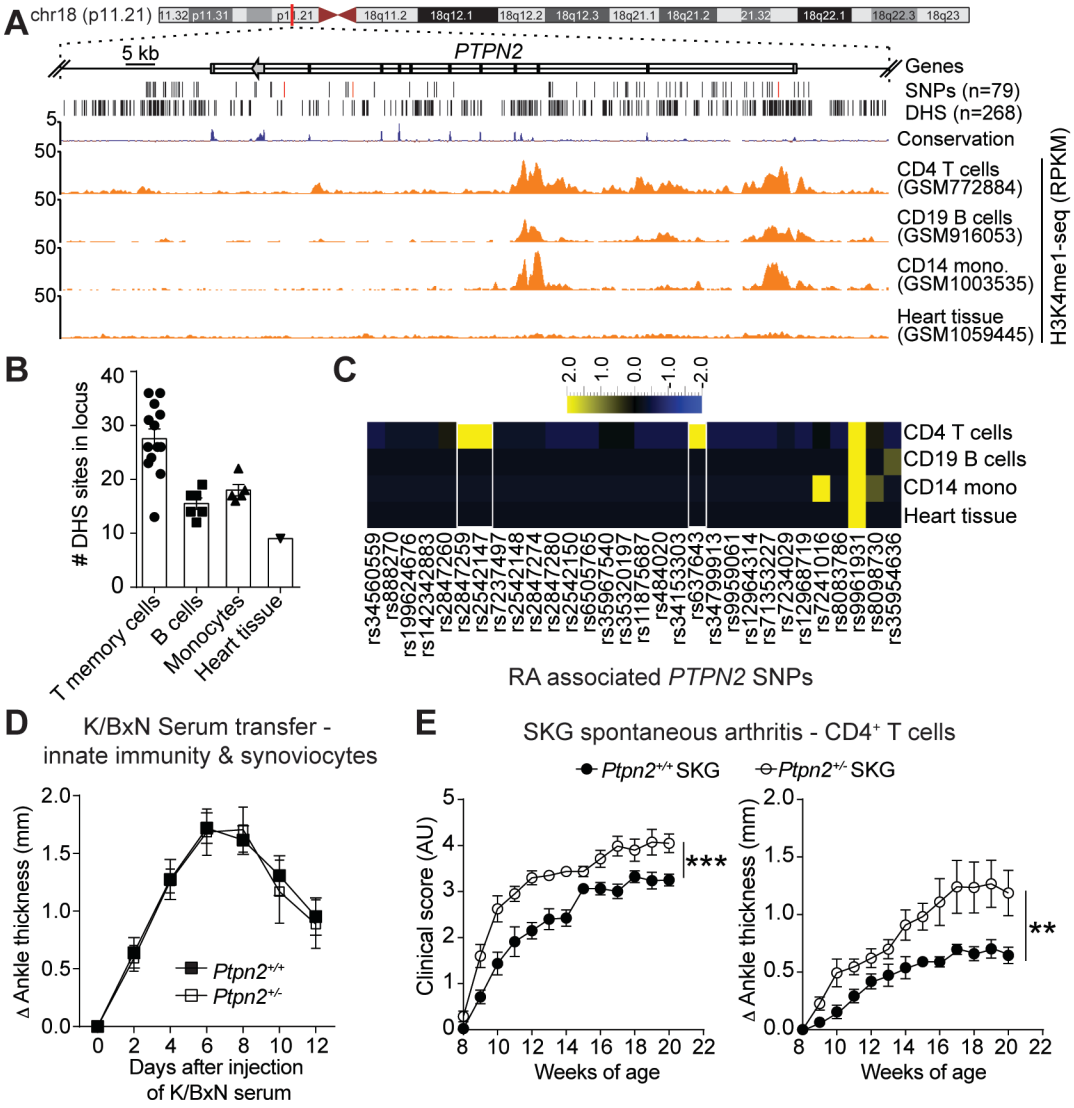

Figure 1. RA-associated haploinsufficiency of *Ptpn2* promotes T cell dependent arthritis in mice. **A**) UCSC tracks showing the chromosomal location of the human *PTPN2* gene, containing a large haplotype block of RA-associated SNPs. Black lines indicate SNPs' genomic location (the characterizing SNPs rs2847297, rs1893217 and rs8083786 are indicated in red), and DNase hypersensitivity sites (DHS). Example tracks of H3K4me1-seq from CD4 T cells, CD19 B cells, CD14 monocytes and heart tissue. **B)** Number of DHS in the *PTPN2* locus in single data sets of 4 primary cell types. **C)** Heat map of RA associated SNPs (columns) that overlap with DHS in different primary cell types (rows). **D)** Development of K/BxN serum-induced arthritis in *Ptpn2*$^{+/+}$ (n=9) and *Ptpn2*$^{+/-}$ (n=7)

male BALB/c mice. **E)** Clinical score (*left panel*) and ankle thickness (*right panel*) during development of spontaneous arthritis in female *Ptpn2*$^{+/+}$ (n=8) and *Ptpn2*$^{+/-}$ (n=8) SKG mice. Compiled data from at least two independent experiments are shown in (**D, E**). Arthritis severity was quantified utilizing the area under the curve. Bars represent mean ± SEM. $^{**}P < 0.01$, $^{***}P < 0.001$ by Mann-Whitney.

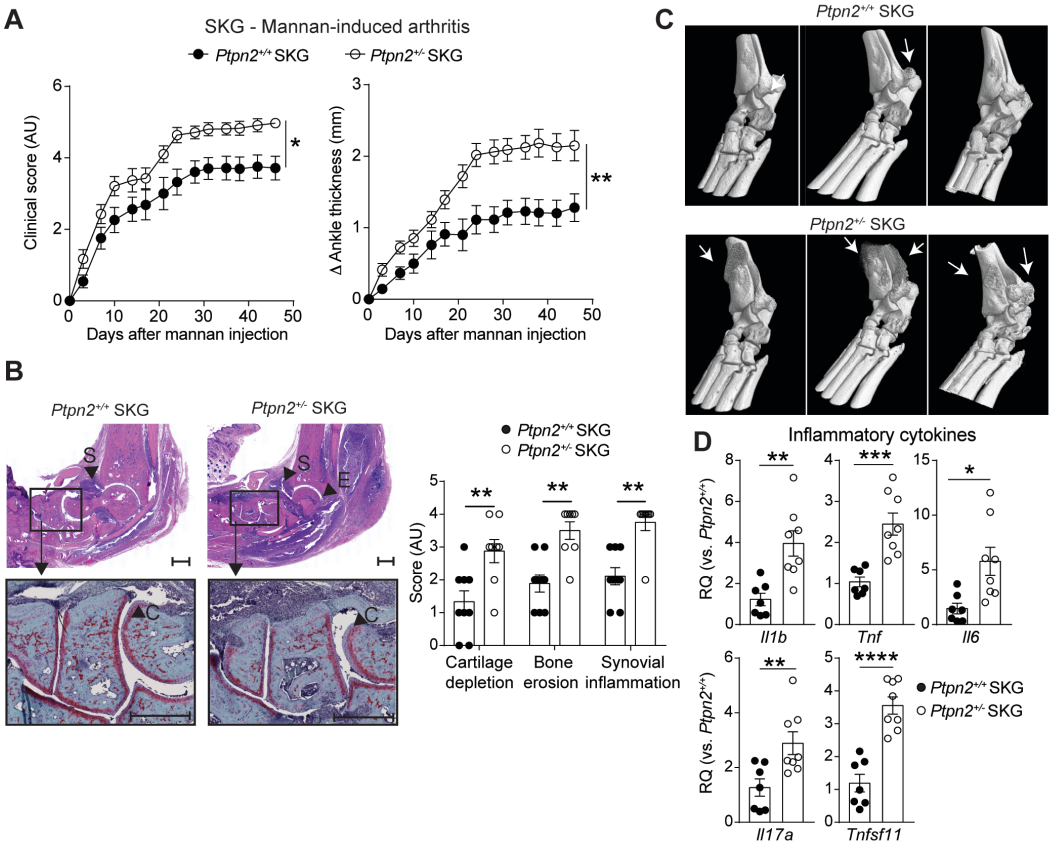

Figure 2. *Ptpn2* haploinsufficiency aggravates mannan-induced arthritis in SKG mice. A) Clinical score (*left panel*) and ankle thickness (*right panel*) in male *Ptpn2*$^{+/+}$ (n=13) and *Ptpn2*$^{+/-}$ (n=11) SKG mice after mannan injection. **B)** Representative images of hematoxylin/eosin (*top left panels*) and safranin-O staining (*lower left panels*) of ankles from *Ptpn2*$^{+/+}$ (n=9) and *Ptpn2*$^{+/-}$ (n=8) SKG mice with mannan induced arthritis. Arrows indicate synovial inflammation (S), bone erosion (E) and cartilage depletion (C), which are quantified in the *right panel*. Scale bar 500 μm. **C)** Micro-CT of arthritic ankles from individual *Ptpn2*$^{+/+}$ and *Ptpn2*$^{+/-}$ male SKG mice with mannan-induced arthritis. White arrows indicate bone erosion or reactive bone deposition that is markedly increased in *Ptpn2*$^{+/-}$ SKG mice. **D)** qPCR analysis of cytokine gene expression in ankles of *Ptpn2*$^{+/+}$ (n=7) and *Ptpn2*$^{+/-}$ (n=8) male SKG mice 35 days after mannan injection. Compiled data from at least two independent experiments are shown in (**A-D**). Arthritis severity was quantified utilizing the area under the curve. Each symbol in (**B, D**) represents

an individual mouse. Bars represent mean ± SEM. *P < 0.05, **P < 0.01, ***P < 0.001, ****P < 0.0001by Mann-Whitney (**A, B**) or unpaired t-test (**D**).

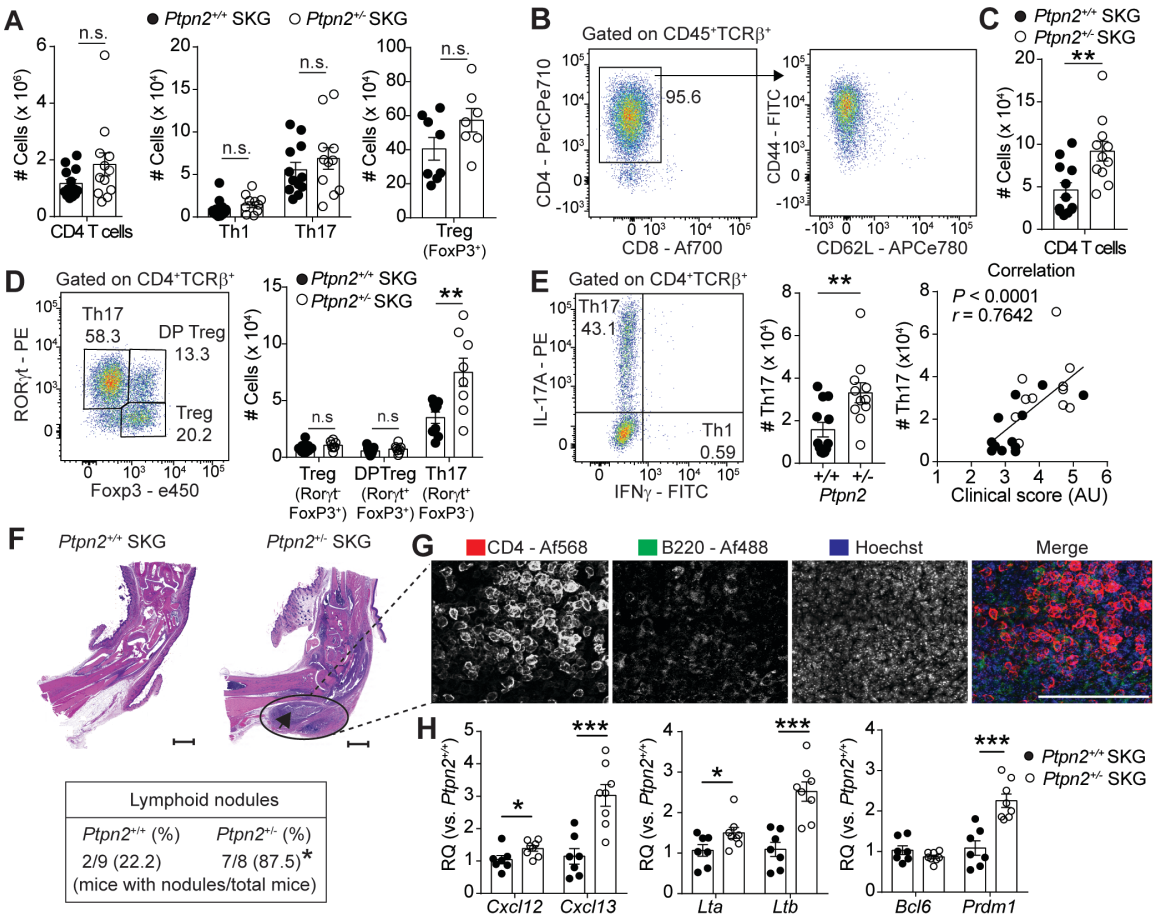

Figure 3. Increased accumulation of synovial Th17 cells and ELS in *Ptpn2* haploinsufficient SKG mice. **A)** Number of CD4 T cells and effector populations Th1, Th17 (*Ptpn2*$^{+/+}$ n=12 and *Ptpn2*$^{+/-}$ n=11) and Tregs (*Ptpn2*$^{+/+}$ n=8 and *Ptpn2*$^{+/-}$ n=7) in popliteal lymph nodes of SKG mice 30-35 days after mannan injection. **B)** Distribution of CD4 and CD8 T cells among TCRβ^{+} T cells (*left panel*) and expression of CD44 and CD62L on CD4 T cells (*right panel*) in arthritic ankles after mannan injection. **C-D)** Number of CD4 T cells in arthritic ankles and Tregs (TCRβ^{+}CD4^{+}FoxP3^{+}RORγt^{-}), RORγt^{+} Tregs (TCRβ^{+}CD4^{+}FoxP3^{+}RORγt^{+}) and Th17 cells (TCRβ^{+}CD4^{+}FoxP3^{-}RORγt^{+}) in ankles of *Ptpn2*$^{+/+}$ (n=9) and *Ptpn2*$^{+/-}$ (n=8) male SKG mice 30-35 days after mannan injection. **E)** Number of Th17 (TCRβ^{+}CD4^{+}IL-17A^{+}IFNγ^{-}; *left panel*) and the correlation between clinical score and number of Th17 within ankles (*right panel,* Spearman correlation) of male

Ptpn2$^{+/+}$ (n=12, filled circles) and *Ptpn2*$^{+/-}$ (n=11, hollow circles) SKG mice 30-35 days after mannan injection. **F)** Representative microscopic image used to assess the presence of ELS (indicated by black arrow, scale bar 500 μm) in male *Ptpn2*$^{+/+}$ and *Ptpn2*$^{+/-}$ SKG mice after mannan injection (**P=0.015*, Fisher's exact test). **G)** Representative 2D Maximum intensity projection of multipanel confocal images of CD4 (red) and B220 (green) in ELS from ankle synovial tissue of male *Ptpn2*$^{+/-}$ SKG mice day 35 after mannan injection. Representative of 3 individual mice. Scale bar 200 μm. **H)** qPCR analysis of ELS-associated gene expression in ankles of male *Ptpn2*$^{+/+}$ (n=7) and *Ptpn2*$^{+/-}$ (n=8) SKG mice 35 days after mannan injection. Compiled data from at least two independent experiments are shown in (**A**-**H**). Each symbol in (**A-H**) represents an individual mouse. Bars represent mean ± SEM. **P* < 0.05, ***P* < 0.01, ****P* < 0.001 by unpaired t-test.

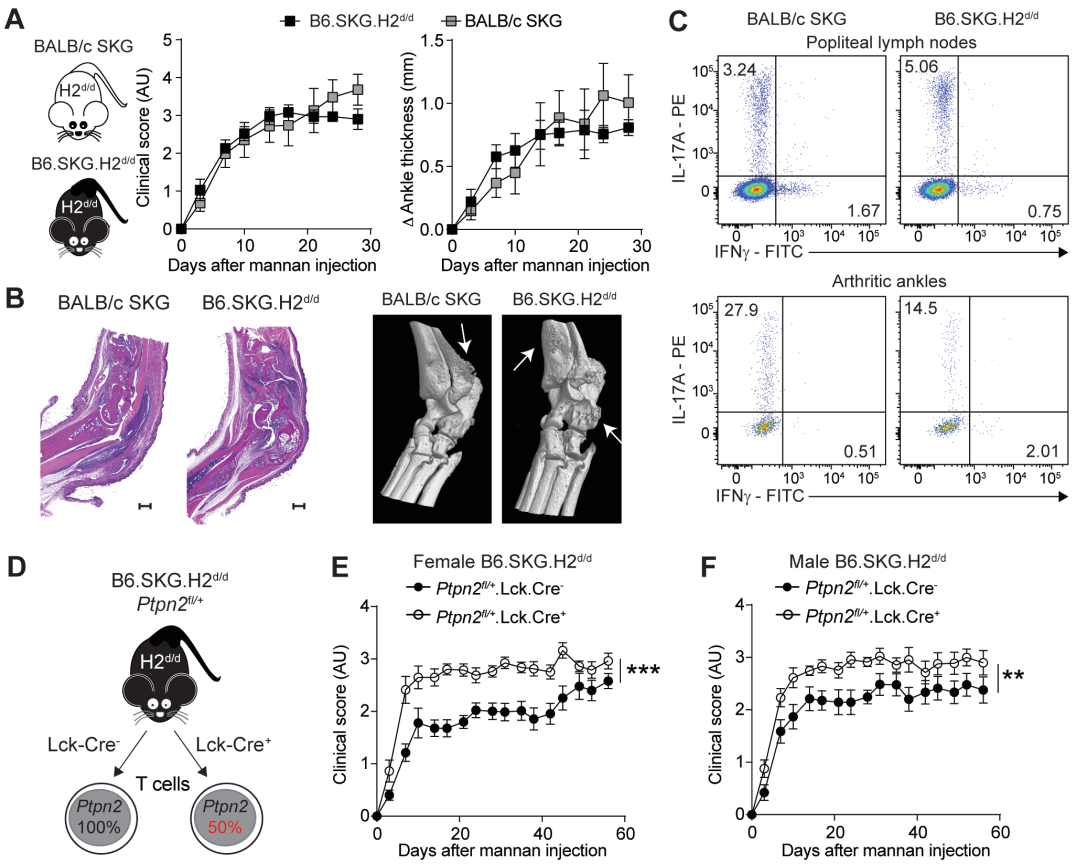

Figure 4. *Ptpn2* haploinsufficiency promotes arthritis through T cells. A) Clinical score (*left panel*) and ankle swelling (*right panel*) in BALB/c SKG (n=6) and B6.SKG.H2$^{d/d}$ (n=6) mice after injection of mannan. **B)** Representative hematoxylin/eosin staining (*left panel,* scale bar 500 μm) and representative micro-CT image (*right panel*) of arthritic ankles from BALB/c SKG and B6.SKG.H2$^{d/d}$ mice. White arrows indicate bone erosion or reactive bone deposition. **C)** Representative flow cytometry staining of Th1 and Th17 in popliteal lymph nodes (*upper panels*) and arthritic ankles (*lower panels*) of BALB/c SKG and B6.SKG.H2$^{d/d}$ mice. **D)** Generation of B6.SKG.H2$^{d/d}$ mice with a T cells specific haploinsufficiency of *Ptpn2*. **E-F**) Clinical score of mannan-induced arthritis in female **(E)** and male **(F)** B6.SKG.H2$^{d/d}$*Ptpn2*$^{fl/+}$Lck-cre^{-} (female n=9; male n=9) and B6.SKG.H2$^{d/d}$*Ptpn2*$^{fl/+}$Lck-cre^{+} (female n=8; male n=9) mice. Compiled data from at least two independent experiments are presented. Arthritis severity was quantified utilizing the area under the curve. Bars represents mean ± SEM. $^{**}P < 0.01$, $^{***}P < 0.001$ by Mann-Whitney.

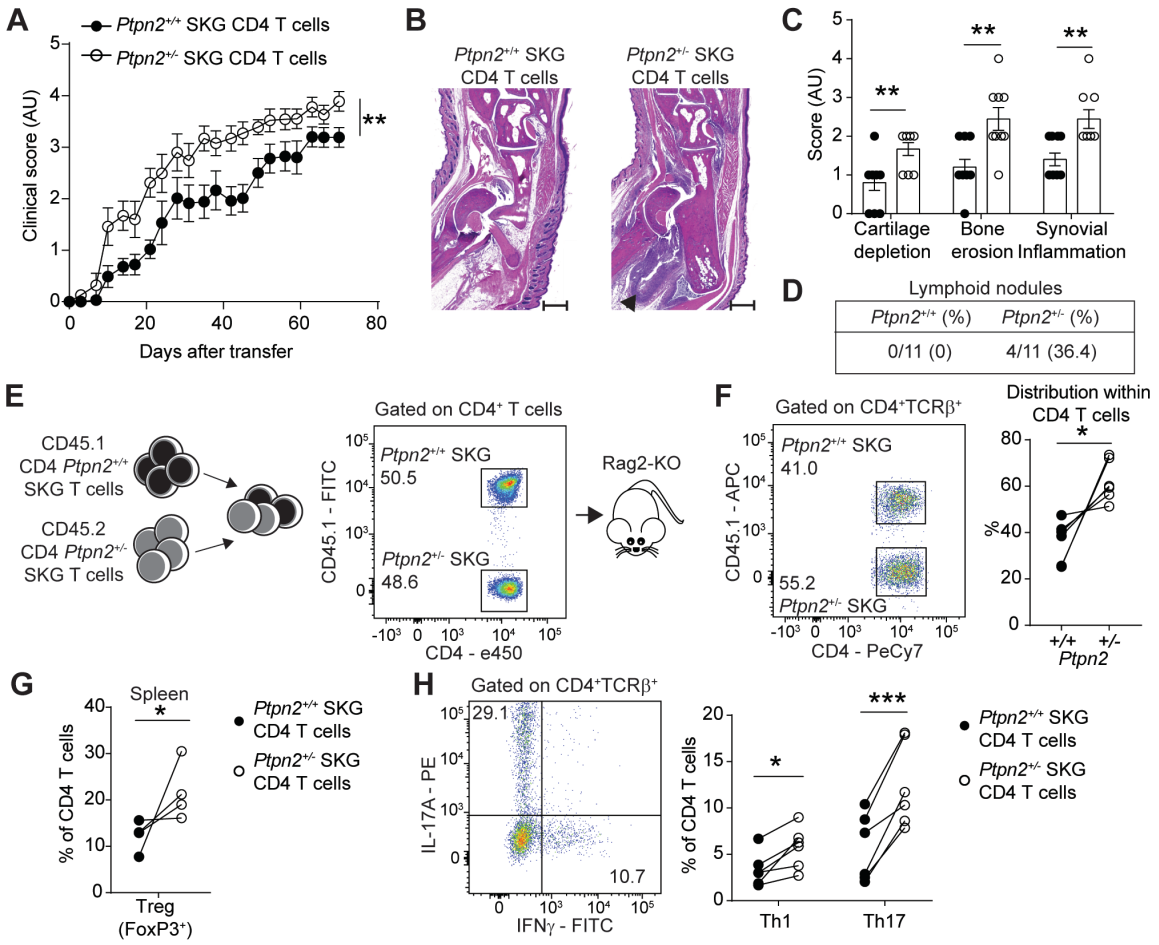

Figure 5. *Ptpn2* haploinsufficient CD4 T cells transfer enhanced arthritis to Rag2-KO mice. A) Clinical scores after transfer of total CD4 SKG T cells isolated from pre-arthritic *Ptpn2*$^{+/+}$ (n=10) and *Ptpn2*$^{+/-}$ (n=10) male SKG mice to male Rag2-KO mice. **B-C)** Representative hematoxylin/eosin staining used for histological evaluation (**B** scale bar 500 μm, quantification shown in **C**) of ankle joints of Rag2-KO mice in **A** (n=10 for each genotype). **D)** Presence of ELS in arthritic ankles of Rag2-KO mice after transfer with CD4 SKG T cells in **A**. **E)** Generation of CD4 SKG T cell chimeras. **F-H)** Analysis of expansion of CD4 T cells (**F**, n=6) and effector populations Th1 and Th17 in lymph nodes (**H**, n=6) and Tregs in the spleen (**G**, n=4) of T cell chimeras during the arthritic phase (12-14 weeks after transfer) in Rag2-KO mice. Compiled data from at least two independent experiments are presented. Each symbol in (**C**-**H**) represents an individual mouse. Arthritis severity was quantified utilizing the area under the curve. Bars represents

mean ± SEM. *P < 0.05, **P < 0.01, ***P < 0.001 by Mann-Whitney **(A, C)** or paired t-test **(F-H).**

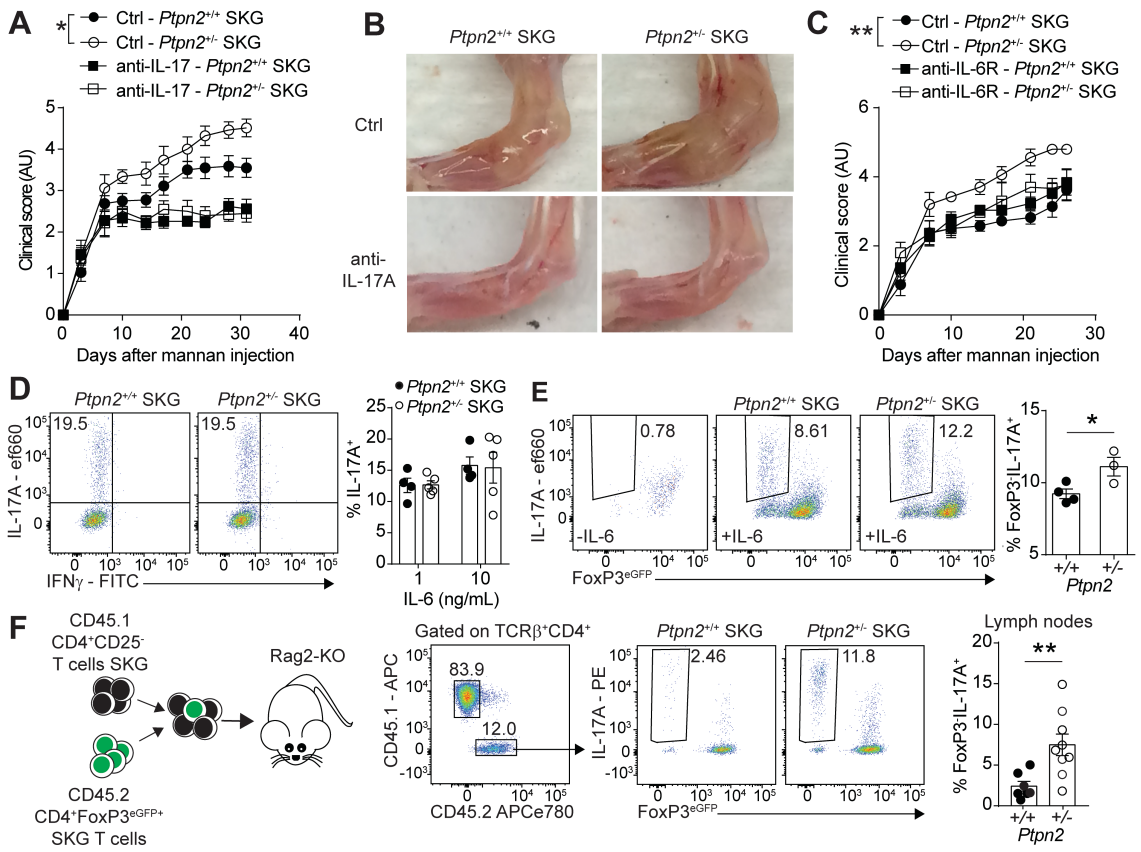

Figure 6. IL-6 promotes arthritis and Treg conversion in *Ptpn2* haploinsufficient mice. A) Clinical score of male SKG mice after treatment with anti-IL-17A antibodies once weekly (100 μg i.p.; *Ptpn2*$^{+/+}$ n=5, *Ptpn2*$^{+/-}$ n=4) or control (*Ptpn2*$^{+/+}$ n=8, *Ptpn2*$^{+/-}$ n=8) during mannan-induced arthritis. **B**) Representative images of ankles of 4 individual *Ptpn2*$^{+/+}$ and *Ptpn2*$^{+/-}$ SKG mice treated anti-IL-17A or control. **C**) Clinical scores of male *Ptpn2*$^{+/+}$ and *Ptpn2*$^{+/-}$ SKG mice treated with anti-IL-6R antibody once weekly (200 μg i.p.; *Ptpn2*$^{+/+}$ n=3, *Ptpn2*$^{+/-}$ n=3) or control (*Ptpn2*$^{+/+}$ n=5, *Ptpn2*$^{+/-}$ n=5) during mannan-induced arthritis. **D**) In vitro differentiation of Th17 cells from naïve *Ptpn2*$^{+/+}$ (n=4) and *Ptpn2*$^{+/-}$ (n=5) SKG CD4 T cells. **E**) Conversion of flow-sorted *Ptpn2*$^{+/+}$ (n=4) and *Ptpn2*$^{+/-}$ (n=3) SKG Tregs (CD4^{+}FoxP3^{eGFP+}) into IL-17 producing exTregs (IL-17A^{+}Foxp3^{eGFP-}) after 72h of stimulation with IL-6 (50ng/mL) and anti-CD3/CD28 coated beads in vitro. **F**) Co-transfer of CD45.1 SKG CD4^{+}CD25^{-} T cells with CD45.2 SKG Tregs to Rag2-KO mice. Transferred CD45.2 *Ptpn2*$^{+/+}$ (n=7) and *Ptpn2*$^{+/-}$ (n=9) SKG Tregs were analyzed in lymph nodes of arthritic mice.

Compiled data from at least two independent experiments are shown. Each symbol in (**D**-**F**) represents an individual mouse. Arthritis severity was quantified utilizing the area under the curve. Bars represent mean ± SEM. **P* < 0.05, ***P* < 0.01 by Mann-Whitney **(A, C)** or un-paired t-test (**E**, **F**).

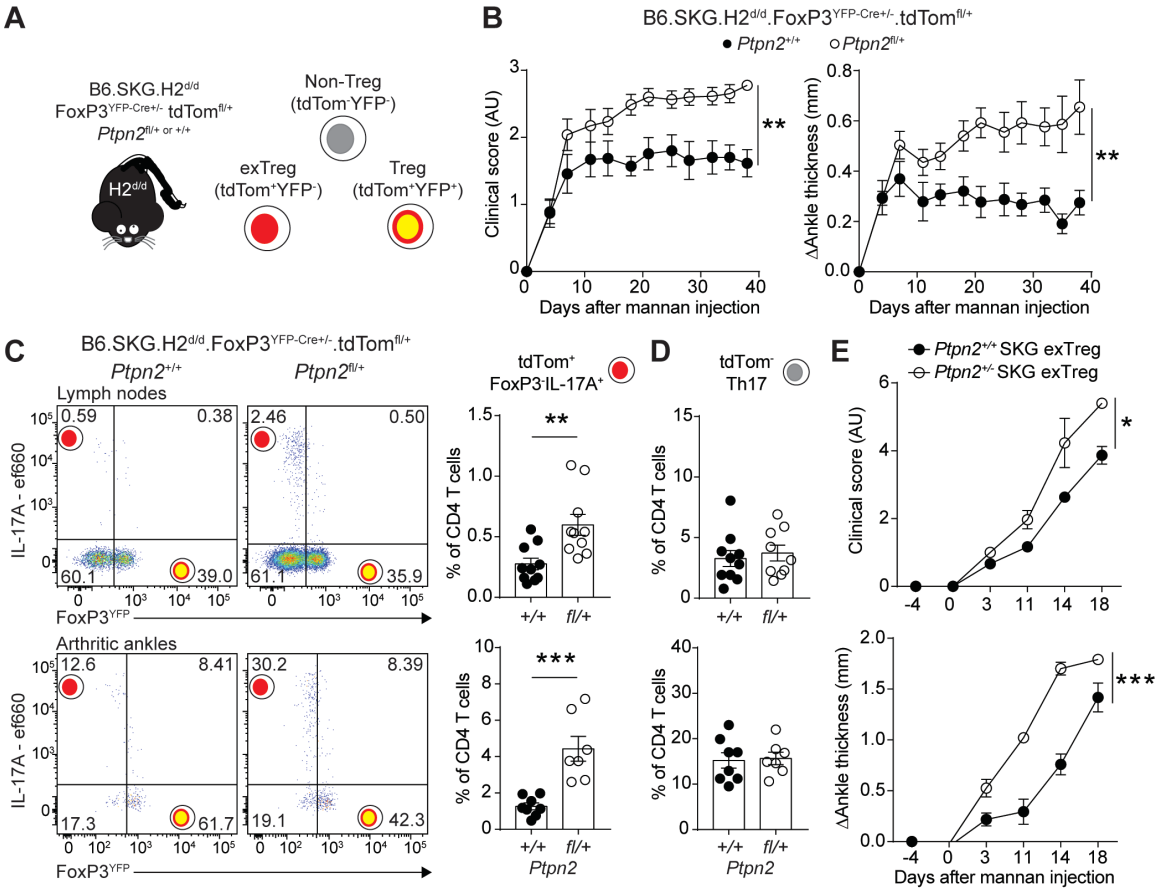

Figure 7. Treg specific *Ptpn2* haploinsufficiency promotes pathogenic Treg conversion and enhances arthritis severity. A) Generation of B6.SKG.H2$^{d/d}$.FoxP3$^{YFP\text{-}cre+/-}$.tdTom$^{fl/+}$.*Ptpn2*$^{fl/+}$ fate mapping mice. **B**) Clinical score (*left panel*) and ankle swelling (*right panel*) of female B6.SKG.H2$^{d/d}$.FoxP3$^{YFP\text{-}cre+/-}$.tdTom$^{fl/+}$.*Ptpn2*$^{+/+}$ (n=8) and *Ptpn2*$^{fl/+}$ (n=8) mice after injection with mannan at 8 weeks of age. **C**) IL-17 expressing cells within TCRβ^{+}CD4^{+}tdTom^{+} cells in lymph nodes (*upper panels,* axillary and popliteal, *Ptpn2*$^{+/+}$ (n=10) and *Ptpn2*$^{fl/+}$ (n=10)) and arthritic ankles (*lower panels, Ptpn2*$^{+/+}$ (n=8) and *Ptpn2*$^{fl/+}$ (n=7)). Flow plots represents frequency within the TCRβ^{+}CD4^{+}tdTom^{+} population. Graphs represent frequency within the total TCRβ^{+}CD4^{+} T cell population. **D**) Frequency of TCRβ^{+}CD4^{+}tdTom^{-} Th17 cells represented as the frequency within the total TCRβ^{+}CD4^{+} T cell population in the same mice as in **C**. **E**) Transfer of in vitro generated *Ptpn2*$^{+/+}$ (n=3) and *Ptpn2*$^{+/-}$

SKG (n=3) eGFP$^-$ exTregs to female Rag2-KO mice ($1.5x10^5$ exTregs/mouse). Arthritis was induced 4 days after transfer by mannan injection. Compiled data from at least three independent experiments are presented in (**B**-**D)**. Experiment in **E** was performed once. Each symbol in (**C, D**) represents an individual mouse. Arthritis severity was quantified utilizing the area under the curve. Bars represent mean ± SEM. $^{**}P < 0.01$, $^{***}P < 0.001$ by Mann-Whitney **(B)** or un-paired t-test (**C, E**).

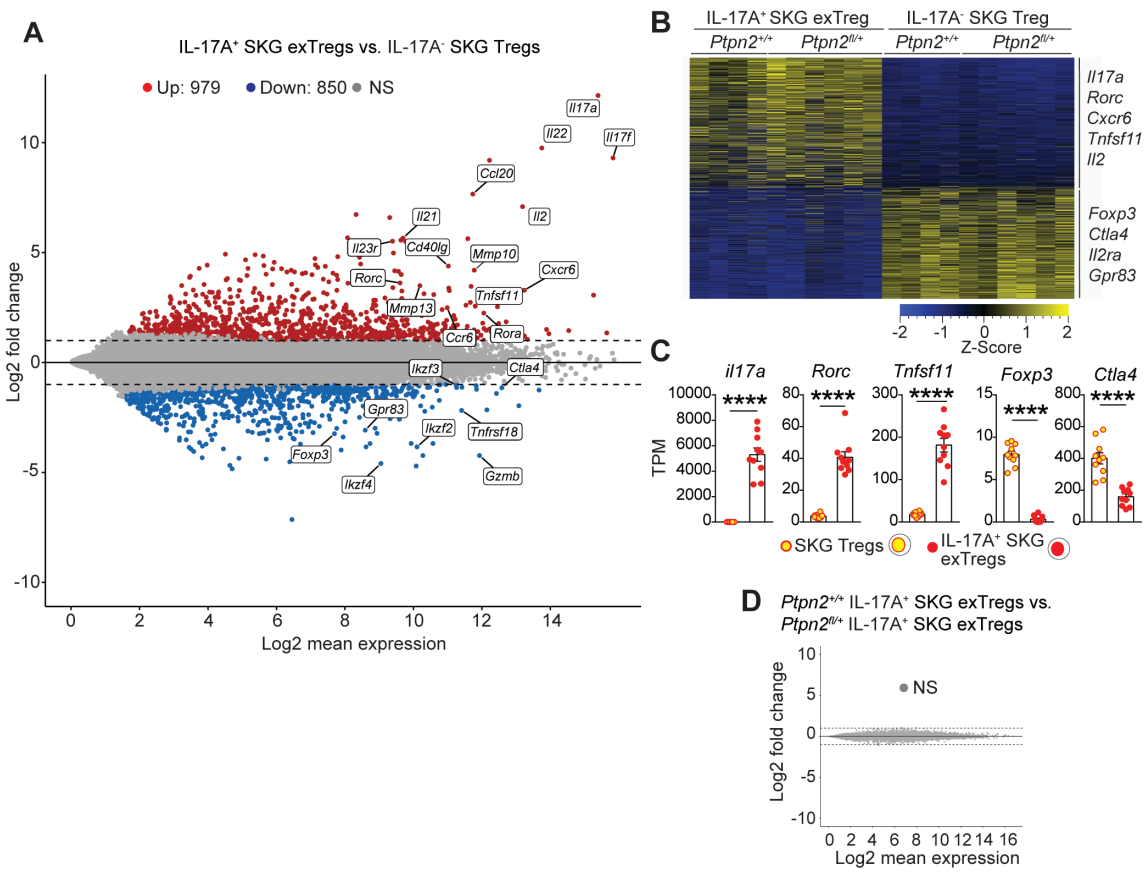

Figure 8. Transcriptomic comparison of in vivo isolated exTregs and Tregs. **A-D**) RNA-Seq performed on IL-17A^{+} SKG exTregs and IL-17^{-} SKG Tregs sorted from *Ptpn2*$^{fl/+}$ (n=6) or *Ptpn2*$^{+/+}$ (n=4) arthritic fate mapping mice. **A**) MD-plot of significantly (*Padj* < 0.05 and fold change > 2) up-regulated (red) and down-regulated (blue) genes in IL-17A^{+} exTregs vs IL-17A^{-} Tregs. Gray represents non-significantly (NS) expressed genes. **B**) Heat-Map of TPM values generated using genes with a fold change > 2 and *Padj* < 0.05. **C)** Normalized expression of selected genes in SKG IL-17A^{+} exTregs and IL-17A^{-} SKG Tregs. **D)** MD-plot comparing *Ptpn2*$^{+/+}$ and *Ptpn2*$^{+/-}$ IL-17A^{+} exTregs**.** Compiled data from at least three independent experiments are presented. Each symbol in (**C**) represents an individual mouse. Bars represent mean ± SEM. ****P < 0.0001 by un-paired t-test (**C**).

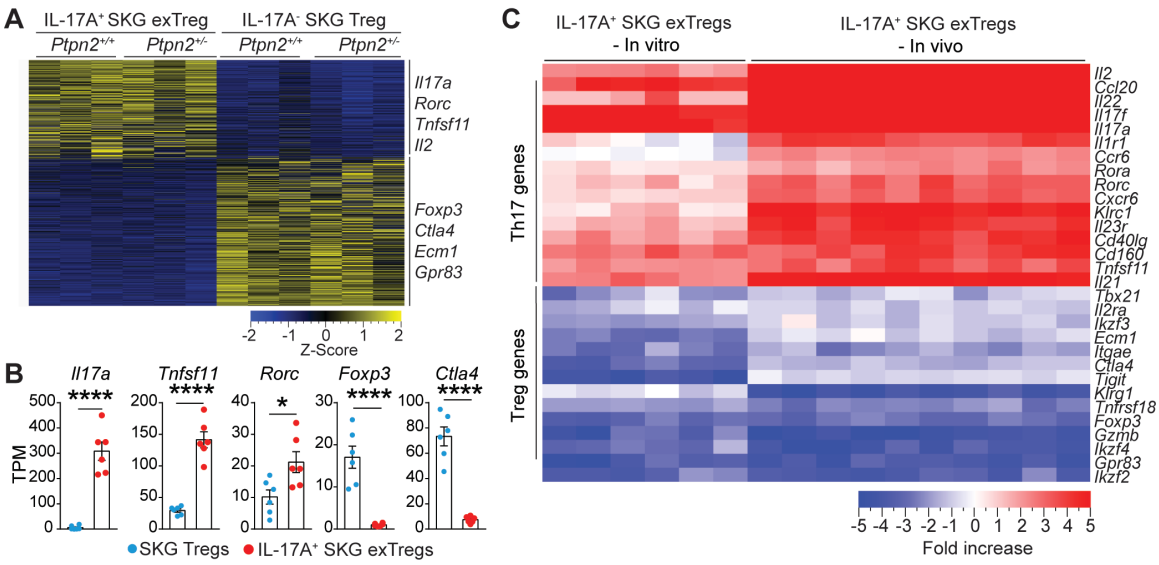

Figure 9. In vitro generated exTregs recapitulate in vivo exTregs. A-C) RNA-Seq analysis performed on IL-17^{+} SKG exTregs and IL-17^{-} SKG Tregs generated in vitro from *Ptpn2*$^{+/+}$ (n=3) and *Ptpn2*$^{+/-}$ (n=3) Tregs isolated from FoxP3^{eGFP} SKG mice and stimulated for 72h hours with IL-6 (50 ng/mL) and anti-CD3/CD28 coated beads. **A)** Heat-Map of TPM values generated using genes with a fold change > 2 and *Padj* < 0.05. **B)** Normalized expression of selected genes in IL-17A^{+} SKG exTregs and IL-17A^{-} SKG Tregs. **C)** Expression of 30 genes associated with the transcriptional profile of Tregs and Th17 cells in in vitro IL-17A^{+} SKG exTregs and in vivo IL-17A^{+} SKG exTregs. Heat-map represents fold change between Tregs and exTregs generated from raw counts. Compiled data from at three independent experiments are presented. Each symbol in (**B**) represents an individual mouse. Bars represent mean ± SEM. **P* < 0.05, *****P* < 0.0001 by un-paired t-test (**B**).

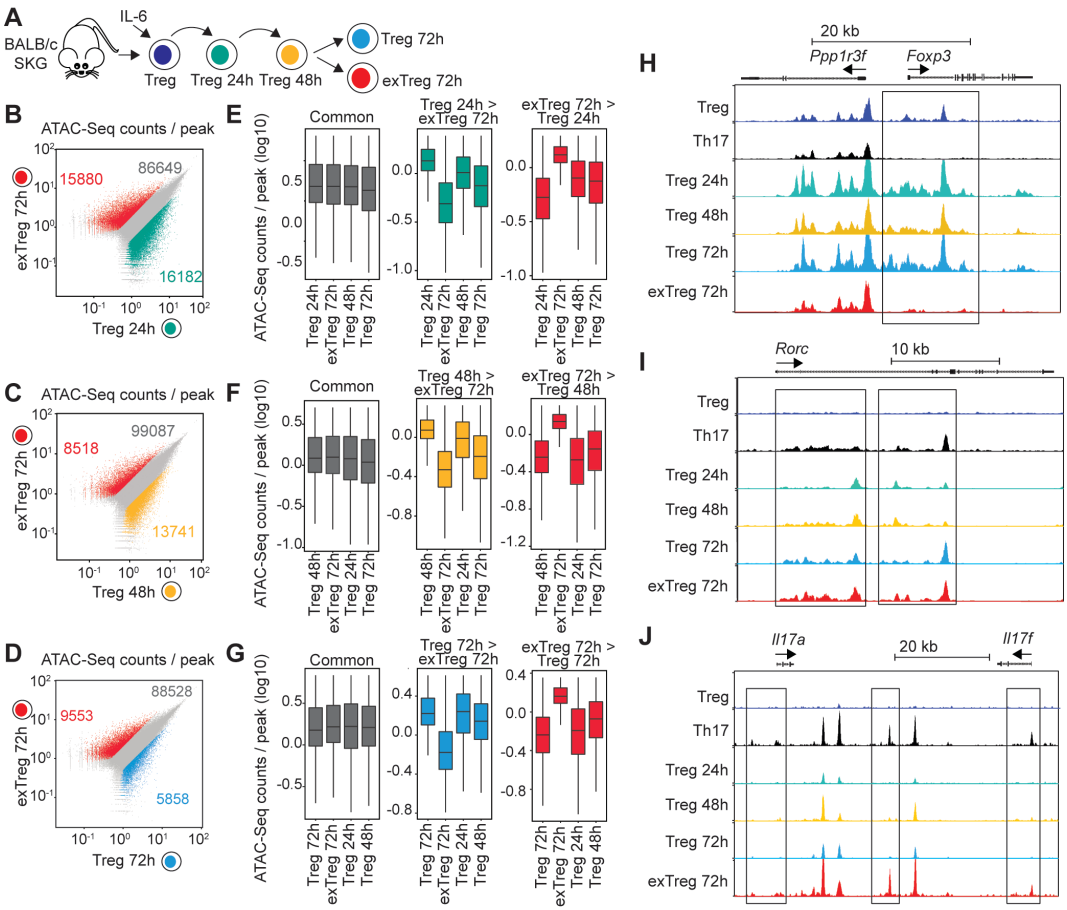

Figure 10. exTregs display a unique chromatin landscape. A-J) ATAC-Seq for chromatin accessibility in SKG Tregs and SKG Th17 cells, as well as SKG Tregs during in vitro conversion and SKG exTregs**. A)** Experimental design for evaluation of chromatin profile in SKG Tregs during in vitro conversion in the presence of IL-6 (50 ng/mL) and anti-CD3/CD28. Tregs were isolated after 24h, 48h and 72h of culture whereas exTregs were isolated after 72h. **B-D)** Scatterplots of ATAC-seq counts per peak comparing indicated samples. **E-G)** Boxplots of ATAC-seq counts per peak from indicated samples at common or differentially accessible regions from the comparison labeled above. Box indicates interquartile range with whiskers 1.5 times this range and outlier points. **H-J)** Normalized ATAC-seq coverage at the *Foxp3* (**H**), *Rorc* (**I**) and the *Il17a* and *Il17f* (**J**) loci in Tregs, Th17 and Tregs during in vitro conversion and exTregs. Scale 0-1200 for *Foxp3* and *Rorc*, 0-800 for *Il17a* and *Il17f*. Black squares represent visually evident changes in ATAC signal. ATAC-seq from two independent replicates.

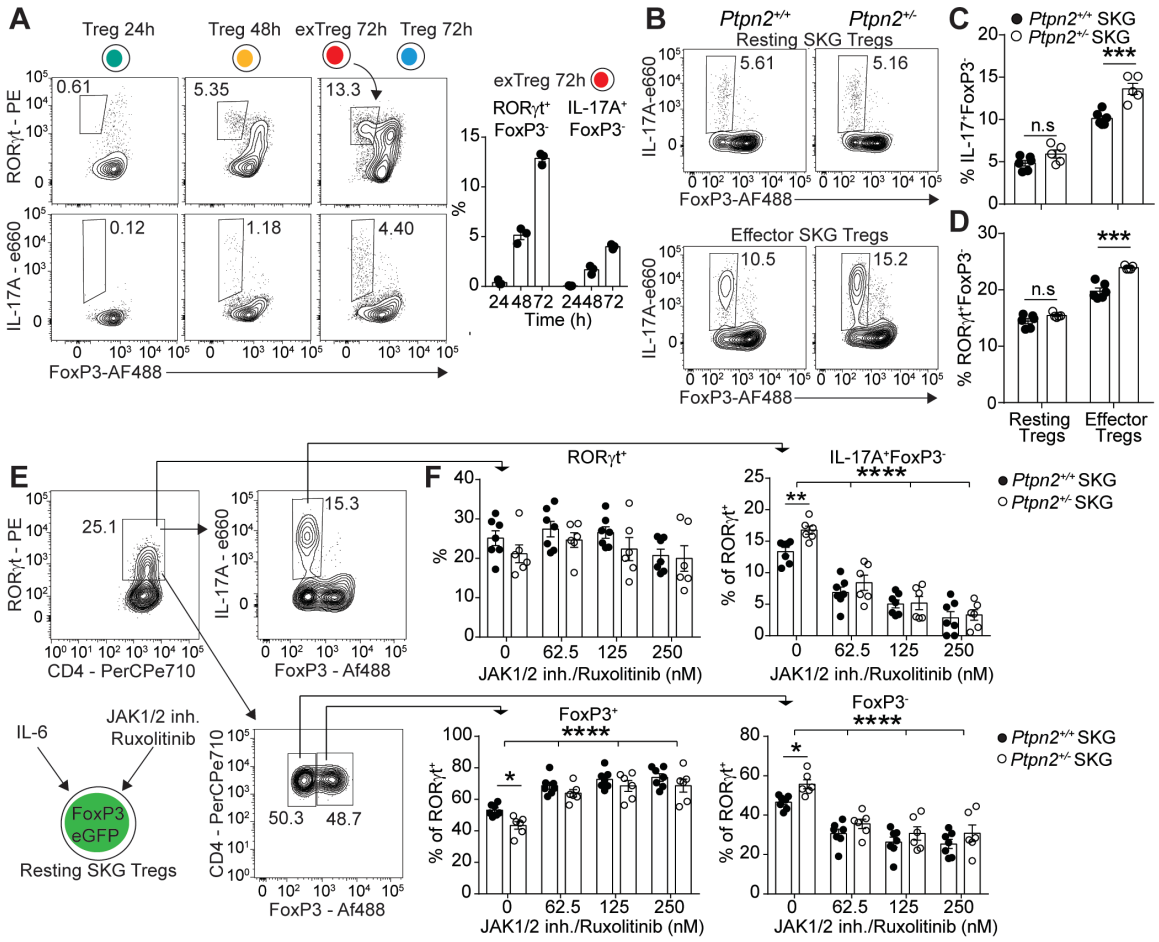

Figure 11. *Ptpn2* haploinsufficiency promotes conversion of RORγt$^+$ effector Tregs. A) Kinetics of IL-17A$^+$ exTregs generation during in vitro stimulation of sorted *Ptpn2*$^{+/+}$ FoxP3^{eGFP} SKG Tregs (n=3) with IL-6 (50 ng/mL) and anti-CD3/CD28 coated beads. **B-C**) In vitro conversion of *Ptpn2*$^{+/+}$ (n=6) and *Ptpn2*$^{+/-}$ (n=5) effector and resting SKG Tregs into IL-17$^+$ exTregs. **D**) Generation of FoxP3$^-$ RORγt$^+$ exTregs (gated as in **A**) from *Ptpn2*$^{+/+}$ and *Ptpn2*$^{+/-}$ effector and resting SKG Tregs. **E-F**) Inhibition of JAK1/2 signaling using Ruxolitinib during in vitro conversion of resting SKG Tregs. **E**) Gating strategy for evaluation of RORγt$^+$ expressing *Ptpn2*$^{+/+}$ (n=7) and *Ptpn2*$^{+/-}$ (n=6) cells after 72h of culture. **F**) Effect of JAK1/2 inhibition on upregulation of RORγt$^+$ on live cells (*upper left panel*), the generation of IL-17$^+$FoxP3$^-$ exTregs (*upper right panel*) and the loss of FoxP3 within the RORγt$^+$ population (*lower panels*). Compiled data from two experiments are presented (**C-F**). Each symbol represents an individual mouse. Bars represent

mean ± SEM. *$P < 0.05$, **$P < 0.01$, ***$P < 0.001$, ****$P < 0.0001$ by un-paired t-test (**C, D**) or 2-way ANOVA (**F**).

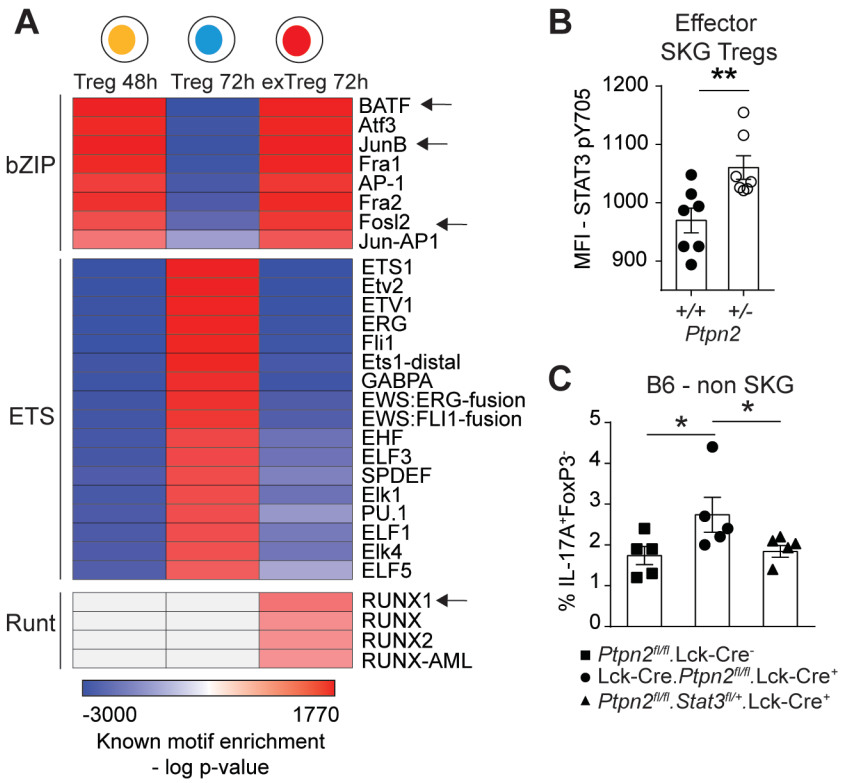

Figure 12. Increased conversion of *Ptpn2* haploinsufficient Tregs is mediated through STAT3. A) Motif enrichment analysis on differentially accessible regions identified by pairwise comparison of Tregs 24h versus Tregs 48h (Treg 48h), Tregs 48h versus Tregs 72h (Treg 72h) and Tregs 72h versus exTreg 72h (exTreg 72h). Arrows indicate transcription factors that have been reported to associate with STAT3 functions in CD4 T cells. Motifs with an enrichment log p value less than -35 and found in 10% or more regions and a fold increase of 2.5 over background were used to generate the heat-map. Motif enrichment analysis performed on ATAC-seq experiment in **Figure 10**. **B**) IL-6 (5 ng/mL) induced activation of STAT3 (pY705) in *Ptpn2*$^{+/+}$ and *Ptpn2*$^{+/-}$ effector SKG Tregs analyzed by flow cytometry. **C**) In vitro conversion of *Ptpn2*$^{fl/fl}$.Lck-Cre^{-} (n=5), *Ptpn2*$^{fl/fl}$.Lck-Cre^{+} (n=5) and *Ptpn2*$^{fl/fl}$*Stat3*$^{fl/+}$.Lck-Cre^{+} (n=5) Tregs isolated from non-SKG B6 mice. Compiled data from two experiments are presented (**B-C**). Each symbol represents in (**B-C**) an individual mouse. Two independent replicates are used for ATAC-Seq heat-map. Bars represent mean ± SEM. *P < 0.05, **P < 0.01, by un-paired t-test (**B**) or Mann-Whitney (**C**).

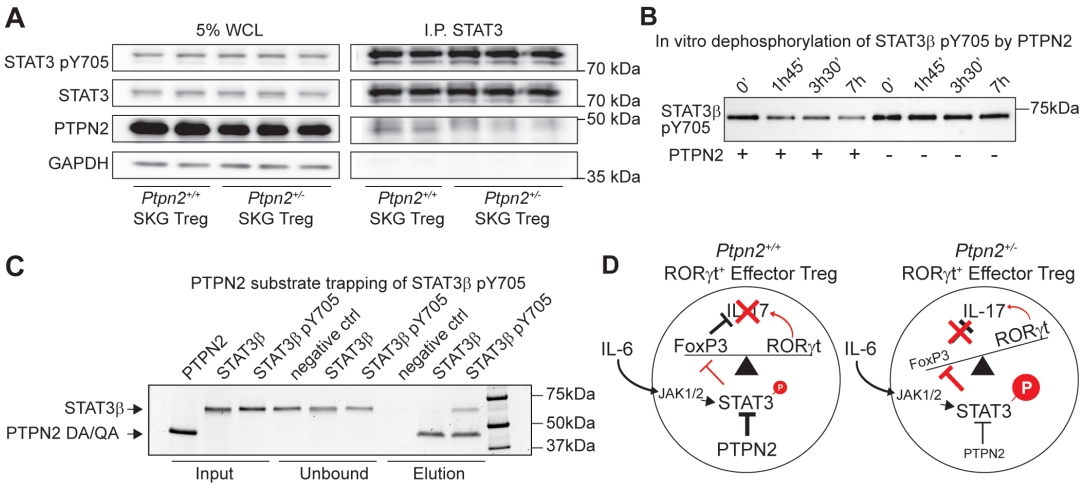

Figure 13. PTPN2 directly interacts and dephosphorylates STAT3. A) Immunoprecipitation of STAT3 in in vitro expanded Tregs (expanded with IL-2 and anti-CD3/CD28 coated beads) after stimulation with IL-6 (50 ng/mL) for 20 minutes. All samples shown were separated on the same gel. WCL = Whole Cell Lysate. **B)** Dephosphorylation of STAT3β pY705 after incubation with (+) or without (-) recombinant PTPN2. Samples were taken at 0, 1h45', 3h30' and 7h for analysis. All samples shown were separated on the same gel. **C**) Substrate trapping of STAT3β pY705 by the PTPN2 mutant (D182A, Q260A). Unphosphorylated Stat3β was used as a negative control and does not bind PTPN2 as shown. Proteins were analyzed by SDS-PAGE and run on the same gel**. D**) Schematic of proposed mechanism by which partial loss of function in PTPN2 in Tregs promotes STAT3 mediated loss of FoxP3 and generation of IL-17A producing exTregs. Representative out of two (**A**) and three (**B, C**) independent experiments are shown.

References

1. McInnes IB, and Schett G. The pathogenesis of rheumatoid arthritis. *N Engl J Med.* 2011;365(23):2205-19.
2. Viatte S, Plant D, and Raychaudhuri S. Genetics and epigenetics of rheumatoid arthritis. *Nat Rev Rheumatol.* 2013;9(3):141-53.
3. Wellcome Trust Case Control C. Genome-wide association study of 14,000 cases of seven common diseases and 3,000 shared controls. *Nature.* 2007;447(7145):661-78.
4. Lees CW, Barrett JC, Parkes M, and Satsangi J. New IBD genetics: common pathways with other diseases. *Gut.* 2011;60(12):1739-53.
5. Long SA, Cerosaletti K, Wan JY, Ho JC, Tatum M, Wei S, Shilling HG, and Buckner JH. An autoimmune-associated variant in PTPN2 reveals an impairment of IL-2R signaling in CD4(+) T cells. *Genes Immun.* 2011;12(2):116-25.
6. Scharl M, Mwinyi J, Fischbeck A, Leucht K, Eloranta JJ, Arikkat J, Pesch T, Kellermeier S, Mair A, Kullak-Ublick GA, et al. Crohn's disease-associated polymorphism within the PTPN2 gene affects muramyl-dipeptide-induced cytokine secretion and autophagy. *Inflamm Bowel Dis.* 2012;18(5):900-12.
7. Doody KM, Bourdeau A, and Tremblay ML. T-cell protein tyrosine phosphatase is a key regulator in immune cell signaling: lessons from the knockout mouse model and implications in human disease. *Immunol Rev.* 2009;228(1):325-41.
8. van Vliet C, Bukczynska PE, Puryer MA, Sadek CM, Shields BJ, Tremblay ML, and Tiganis T. Selective regulation of tumor necrosis factor-induced Erk signaling by Src family kinases and the T cell protein tyrosine phosphatase. *Nat Immunol.* 2005;6(3):253-60.
9. Wiede F, Shields BJ, Chew SH, Kyparissoudis K, van Vliet C, Galic S, Tremblay ML, Russell SM, Godfrey DI, and Tiganis T. T cell protein tyrosine phosphatase attenuates T cell signaling to maintain tolerance in mice. *J Clin Invest.* 2011;121(12):4758-74.
10. Wiede F, Dudakov JA, Lu KH, Dodd GT, Butt T, Godfrey DI, Strasser A, Boyd RL, and Tiganis T. PTPN2 regulates T cell lineage commitment and alphabeta versus gammadelta specification. *J Exp Med.* 2017;214(9):2733-58.
11. Wiede F, Sacirbegovic F, Leong YA, Yu D, and Tiganis T. PTPN2-deficiency exacerbates T follicular helper cell and B cell responses and promotes the development of autoimmunity. *J Autoimmun.* 2017;76(85-100.
12. You-Ten KE, Muise ES, Itie A, Michaliszyn E, Wagner J, Jothy S, Lapp WS, and Tremblay ML. Impaired bone marrow microenvironment and immune function in T cell protein tyrosine phosphatase-deficient mice. *J Exp Med.* 1997;186(5):683-93.
13. Spalinger MR, Kasper S, Chassard C, Raselli T, Frey-Wagner I, Gottier C, Lang S, Atrott K, Vavricka SR, Mair F, et al. PTPN2 controls differentiation of CD4(+) T cells and limits intestinal inflammation and intestinal dysbiosis. *Mucosal Immunol.* 2015;8(4):918-29.

14. Sakaguchi S, Yamaguchi T, Nomura T, and Ono M. Regulatory T cells and immune tolerance. *Cell.* 2008;133(5):775-87.
15. Rudensky AY. Regulatory T cells and Foxp3. *Immunol Rev.* 2011;241(1):260-8.
16. Bothur E, Raifer H, Haftmann C, Stittrich AB, Brustle A, Brenner D, Bollig N, Bieringer M, Kang CH, Reinhard K, et al. Antigen receptor-mediated depletion of FOXP3 in induced regulatory T-lymphocytes via PTPN2 and FOXO1. *Nat Commun.* 2015;6(8576.
17. Schmiedel BJ, Seumois G, Samaniego-Castruita D, Cayford J, Schulten V, Chavez L, Ay F, Sette A, Peters B, and Vijayanand P. 17q21 asthma-risk variants switch CTCF binding and regulate IL-2 production by T cells. *Nat Commun.* 2016;7(13426.
18. Aradi B, Kato M, Filkova M, Karouzakis E, Klein K, Scharl M, Kolling C, Michel BA, Gay RE, Buzas EI, et al. Protein tyrosine phosphatase nonreceptor type 2: an important regulator of Interleukin-6 production in rheumatoid arthritis synovial fibroblasts. *Arthritis Rheumatol.* 2015;67(10):2624-33.
19. Lee DM, Kiener HP, Agarwal SK, Noss EH, Watts GF, Chisaka O, Takeichi M, and Brenner MB. Cadherin-11 in synovial lining formation and pathology in arthritis. *Science.* 2007;315(5814):1006-10.
20. Ji H, Ohmura K, Mahmood U, Lee DM, Hofhuis FM, Boackle SA, Takahashi K, Holers VM, Walport M, Gerard C, et al. Arthritis critically dependent on innate immune system players. *Immunity.* 2002;16(2):157-68.
21. Nandakumar KS, Svensson L, and Holmdahl R. Collagen type II-specific monoclonal antibody-induced arthritis in mice: description of the disease and the influence of age, sex, and genes. *Am J Pathol.* 2003;163(5):1827-37.
22. Kagari T, Doi H, and Shimozato T. The importance of IL-1 beta and TNF-alpha, and the noninvolvement of IL-6, in the development of monoclonal antibody-induced arthritis. *J Immunol.* 2002;169(3):1459-66.
23. Hashimoto M, Hirota K, Yoshitomi H, Maeda S, Teradaira S, Akizuki S, Prieto-Martin P, Nomura T, Sakaguchi N, Kohl J, et al. Complement drives Th17 cell differentiation and triggers autoimmune arthritis. *J Exp Med.* 2010;207(6):1135-43.
24. Sakaguchi N, Takahashi T, Hata H, Nomura T, Tagami T, Yamazaki S, Sakihama T, Matsutani T, Negishi I, Nakatsuru S, et al. Altered thymic T-cell selection due to a mutation of the ZAP-70 gene causes autoimmune arthritis in mice. *Nature.* 2003;426(6965):454-60.
25. Hata H, Sakaguchi N, Yoshitomi H, Iwakura Y, Sekikawa K, Azuma Y, Kanai C, Moriizumi E, Nomura T, Nakamura T, et al. Distinct contribution of IL-6, TNF-alpha, IL-1, and IL-10 to T cell-mediated spontaneous autoimmune arthritis in mice. *J Clin Invest.* 2004;114(4):582-8.
26. Pitzalis C, Kelly S, and Humby F. New learnings on the pathophysiology of RA from synovial biopsies. *Curr Opin Rheumatol.* 2013;25(3):334-44.
27. Grogan JL, and Ouyang W. A role for Th17 cells in the regulation of tertiary lymphoid follicles. *Eur J Immunol.* 2012;42(9):2255-62.

28. Jones GW, Bombardieri M, Greenhill CJ, McLeod L, Nerviani A, Rocher-Ros V, Cardus A, Williams AS, Pitzalis C, Jenkins BJ, et al. Interleukin-27 inhibits ectopic lymphoid-like structure development in early inflammatory arthritis. *J Exp Med.* 2015;212(11):1793-802.
29. Wiede F, La Gruta NL, and Tiganis T. PTPN2 attenuates T-cell lymphopenia-induced proliferation. *Nat Commun.* 2014;5(3073.
30. Liao W, Lin JX, Wang L, Li P, and Leonard WJ. Modulation of cytokine receptors by IL-2 broadly regulates differentiation into helper T cell lineages. *Nat Immunol.* 2011;12(6):551-9.
31. Hirota K, Hashimoto M, Yoshitomi H, Tanaka S, Nomura T, Yamaguchi T, Iwakura Y, Sakaguchi N, and Sakaguchi S. T cell self-reactivity forms a cytokine milieu for spontaneous development of IL-17+ Th cells that cause autoimmune arthritis. *J Exp Med.* 2007;204(1):41-7.
32. Bettelli E, Carrier Y, Gao W, Korn T, Strom TB, Oukka M, Weiner HL, and Kuchroo VK. Reciprocal developmental pathways for the generation of pathogenic effector TH17 and regulatory T cells. *Nature.* 2006;441(7090):235-8.
33. Komatsu N, Okamoto K, Sawa S, Nakashima T, Oh-hora M, Kodama T, Tanaka S, Bluestone JA, and Takayanagi H. Pathogenic conversion of Foxp3+ T cells into TH17 cells in autoimmune arthritis. *Nat Med.* 2014;20(1):62-8.
34. Korn T, Bettelli E, Oukka M, and Kuchroo VK. IL-17 and Th17 Cells. *Annu Rev Immunol.* 2009;27(485-517.
35. Ciofani M, Madar A, Galan C, Sellars M, Mace K, Pauli F, Agarwal A, Huang W, Parkhurst CN, Muratet M, et al. A validated regulatory network for Th17 cell specification. *Cell.* 2012;151(2):289-303.
36. Sugimoto N, Oida T, Hirota K, Nakamura K, Nomura T, Uchiyama T, and Sakaguchi S. Foxp3-dependent and -independent molecules specific for CD25+CD4+ natural regulatory T cells revealed by DNA microarray analysis. *Int Immunol.* 2006;18(8):1197-209.
37. Ohnmacht C, Park JH, Cording S, Wing JB, Atarashi K, Obata Y, Gaboriau-Routhiau V, Marques R, Dulauroy S, Fedoseeva M, et al. MUCOSAL IMMUNOLOGY. The microbiota regulates type 2 immunity through RORgammat(+) T cells. *Science.* 2015;349(6251):989-93.
38. Sefik E, Geva-Zatorsky N, Oh S, Konnikova L, Zemmour D, McGuire AM, Burzyn D, Ortiz-Lopez A, Lobera M, Yang J, et al. MUCOSAL IMMUNOLOGY. Individual intestinal symbionts induce a distinct population of RORgamma(+) regulatory T cells. *Science.* 2015;349(6251):993-7.
39. Quintas-Cardama A, Vaddi K, Liu P, Manshouri T, Li J, Scherle PA, Caulder E, Wen X, Li Y, Waeltz P, et al. Preclinical characterization of the selective JAK1/2 inhibitor INCB018424: therapeutic implications for the treatment of myeloproliferative neoplasms. *Blood.* 2010;115(15):3109-17.
40. Fridman JS, Scherle PA, Collins R, Burn T, Neilan CL, Hertel D, Contel N, Haley P, Thomas B, Shi J, et al. Preclinical evaluation of local JAK1 and JAK2 inhibition in cutaneous inflammation. *J Invest Dermatol.* 2011;131(9):1838-44.

41. Schraml BU, Hildner K, Ise W, Lee WL, Smith WA, Solomon B, Sahota G, Sim J, Mukasa R, Cemerski S, et al. The AP-1 transcription factor Batf controls T(H)17 differentiation. *Nature.* 2009;460(7253):405-9.
42. Mouly E, Chemin K, Nguyen HV, Chopin M, Mesnard L, Leite-de-Moraes M, Burlen-defranoux O, Bandeira A, and Bories JC. The Ets-1 transcription factor controls the development and function of natural regulatory T cells. *J Exp Med.* 2010;207(10):2113-25.
43. Rudra D, deRoos P, Chaudhry A, Niec RE, Arvey A, Samstein RM, Leslie C, Shaffer SA, Goodlett DR, and Rudensky AY. Transcription factor Foxp3 and its protein partners form a complex regulatory network. *Nat Immunol.* 2012;13(10):1010-9.
44. Zhang F, Meng G, and Strober W. Interactions among the transcription factors Runx1, RORgammat and Foxp3 regulate the differentiation of interleukin 17-producing T cells. *Nat Immunol.* 2008;9(11):1297-306.
45. Durant L, Watford WT, Ramos HL, Laurence A, Vahedi G, Wei L, Takahashi H, Sun HW, Kanno Y, Powrie F, et al. Diverse targets of the transcription factor STAT3 contribute to T cell pathogenicity and homeostasis. *Immunity.* 2010;32(5):605-15.
46. Doody KM, Bussieres-Marmen S, Li A, Paquet M, Henderson JE, and Tremblay ML. T cell protein tyrosine phosphatase deficiency results in spontaneous synovitis and subchondral bone resorption in mice. *Arthritis Rheum.* 2012;64(3):752-61.
47. Yi Z, Lin WW, Stunz LL, and Bishop GA. The adaptor TRAF3 restrains the lineage determination of thymic regulatory T cells by modulating signaling via the receptor for IL-2. *Nat Immunol.* 2014;15(9):866-74.
48. Zhou X, Bailey-Bucktrout SL, Jeker LT, Penaranda C, Martinez-Llordella M, Ashby M, Nakayama M, Rosenthal W, and Bluestone JA. Instability of the transcription factor Foxp3 leads to the generation of pathogenic memory T cells in vivo. *Nat Immunol.* 2009;10(9):1000-7.
49. Bussieres-Marmen S, Vinette V, Gungabeesoon J, Aubry I, Perez-Quintero LA, and Tremblay ML. Loss of T-cell protein tyrosine phosphatase in the intestinal epithelium promotes local inflammation by increasing colonic stem cell proliferation. *Cell Mol Immunol.* 2017.
50. Rubtsov YP, Rasmussen JP, Chi EY, Fontenot J, Castelli L, Ye X, Treuting P, Siewe L, Roers A, Henderson WR, Jr., et al. Regulatory T cell-derived interleukin-10 limits inflammation at environmental interfaces. *Immunity.* 2008;28(4):546-58.
51. Madisen L, Zwingman TA, Sunkin SM, Oh SW, Zariwala HA, Gu H, Ng LL, Palmiter RD, Hawrylycz MJ, Jones AR, et al. A robust and high-throughput Cre reporting and characterization system for the whole mouse brain. *Nat Neurosci.* 2010;13(1):133-40.
52. Lin W, Haribhai D, Relland LM, Truong N, Carlson MR, Williams CB, and Chatila TA. Regulatory T cell development in the absence of functional Foxp3. *Nat Immunol.* 2007;8(4):359-68.
53. Monach PA, Mathis D, and Benoist C. The K/BxN arthritis model. *Curr Protoc Immunol.* 2008;Chapter 15(Unit 15 22.